NASA TR R-52

NATIONAL AERONAUTICS AND SPACE ADMINISTRATION

TECHNICAL REPCRT
R-52

SIMILARITY OF FAR NOISE FIELDS OF JETS

By WALTON L. HOWES

1960

For sale by the Superintendent of Documents, U.S. Government Printing Office, Washington 25, D.C. Yearly subscription, $15; foreign, $19; single copy price varies according to size - - - - - - - - - Price 50 cents

TECHNICAL REPORT R-52

SIMILARITY OF FAR NOISE FIELDS OF JETS

By WALTON L. HOWES

Lewis Research Center
Cleveland, Ohio

TECHNICAL REPORT R–52

SIMILARITY OF FAR NOISE FIELDS OF JETS

By Walton L. Howes

SUMMARY

Similarity parameters for far-field noise from jets are derived. For subsonic jets, total acoustic power and acoustic directivity are expressed in terms of the geometric and fluid properties by means of Lighthill's theory of aerodynamic noise. The acoustic-power spectrum and local mean-square-pressure spectrum are expressed in dimensionless form by considering only the definition of spectrum and the primary geometric and fluid properties.

For supersonic jets, the subsonic formulas are modified to include the noise contribution from the supersonic region. This contribution is related to the geometric and flow properties by applying Ribner's theory of near-field noise caused by shock-turbulence interaction.

Only jets issuing from circular nozzles were considered. On the basis of new as well as previous data, all correlations for subsonic jets were generally good. The optimum value of the acoustic-power coefficient was found to be 3×10^{-5}. Correlations for directivity and spectra are presented in graphical form. A slight difference between dimensionless power spectra for large and small jets was noted. Large differences between jet and ambient temperatures produced small effects on power spectra and directivity but had no apparent effect on total power. Pressure probability-densities were approximately normally distributed.

Results for supersonic jets were generally similar to those for subsonic jets. However, the validity of the derived total-power expression is questionable and requires further investigation.

The correlations presented should be useful for engineering purposes.

INTRODUCTION

In connection with the problems created by the effects of jet noise on humans and aircraft structures, the prediction of jet noise fields is of considerable interest. The possibility of predicting characteristics of jet noise fields results as an immediate consequence of measuring those fields. However, although the literature on jet noise includes considerable data, only a small portion of these data has been presented in correlated form. Some of the available data has been summarized in reference 1. However, more general correlating parameters have been applied in references 2 and 3.

The significant variables relating the characteristics of subsonic jets to the radiated noise are indicated by Lighthill's theory of aerodynamic noise (refs. 4 and 5). No corresponding theory exists for supersonic jets. At least for the subsonic case, most of the significant dimensionless groups are indicated in, or are readily derivable from, the theory of reference 4.

It is the purpose of the present report to indicate and attempt to verify jet noise similarity laws on the basis of both new and previously reported data. In this report, all results are restricted to the acoustic far field and to jet nozzle exits having circular cross sections. Both subsonic and supersonic jets are considered.

The correlations obtained should be useful for engineering purposes.

ACOUSTIC SIMILARITY RELATIONS

The acoustic intensity $\vec{I}(\vec{z})$ at distance $\vec{z}$ from a noise source is given by

$$\vec{I}(\vec{z})=\overline{p'(\vec{z})v_n(\vec{z})} \tag{1}$$

where v_n is the normal component of acoustic particle velocity through a control surface of area ds. (All symbols are defined in appendix A.) The time average (denoted by the bar) for

practical purposes need only be taken for a period several times greater than the period associated with the lowest acoustic frequency of interest. The total radiated acoustic power W is given by

$$W=\int_S \vec{I}(\vec{z})\,ds \tag{2}$$

where S is the total area of a control surface enclosing the noise source. In the acoustic far field, that is, in the region surrounding an acoustic source at a distance large compared with an acoustic wavelength, and at distances which are large compared with the extent of the source, the intensity is given to good approximation by the relation

$$\vec{I}(\vec{z})=\frac{\overline{p'^2}(\vec{z})}{\rho_0 a_0} \tag{3}$$

which allows computation of W from acoustic-pressure measurements alone. Equations (1) to (3) are independent of the character of the noise source.

TOTAL POWER

In a theoretical study of aerodynamic noise, Lighthill (ref. 4) found that in the far field the radiated density fluctuations ρ' associated with low-Mach-number turbulence embedded in a quiescent atmosphere were, in the absence of solid boundaries, representable in terms of the fluid variables by

$$\rho'(\vec{x})\approx\frac{1}{4\pi a_0^2}\frac{x_i x_j}{x^3}\int\left[\frac{1}{a_0^2}\frac{\partial^2}{\partial t^2}T_{ij}\right]\left(\vec{y},t-\frac{|\vec{x}-\vec{y}|}{a_0}\right)d\vec{y} \tag{4}$$

where x_i and y_i are coordinates of the observation point and field points, respectively, and the integration is over-all space. The relation between the various coordinates is shown in figure 1. On the basis of certain assumptions regarding the turbulence, Lighthill showed (ref. 4, cf. appendix B also) that, by analyzing the dimensions of equation (4), the total radiated acoustic power is given by

$$W=K\rho_0 A U^8/a_0^5=KL \tag{5}$$

where U is a characteristic jet velocity (cf. appendix C), K is an acoustic-power coefficient, and $L=\rho_0 A U^8/a_0^5$ is the so-called Lighthill parameter. As defined in equation (5), K is $4/\pi$ times K as

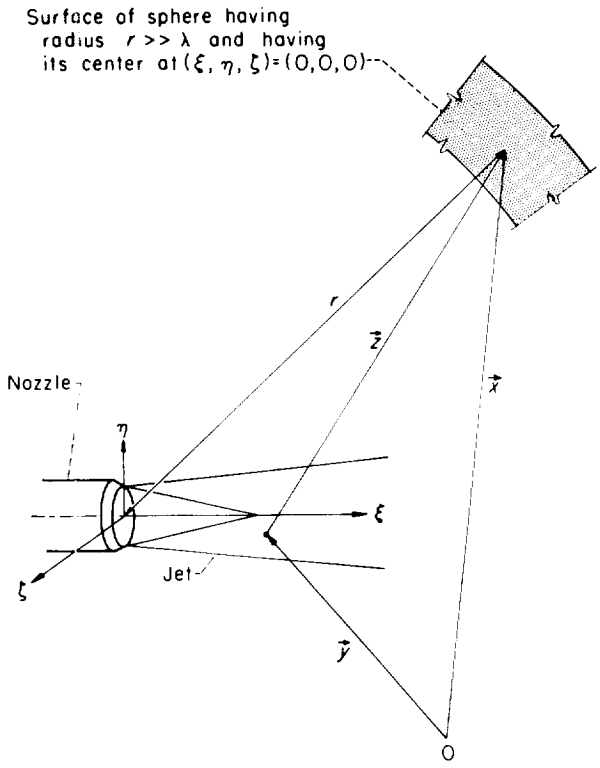

FIGURE 1.—Coordinate systems.

defined by Lighthill. Equation (5) has been found valid for subsonic jets. It is not intended to apply for jets which attain supersonic velocity, especially those containing strong shock waves.

In references 2 (fig. 44) and 3, the acoustic-power output of rockets was empirically correlated in terms of jetstream mechanical power.

The following represents an alternate attempt to relate the far-field acoustic characteristics to the flow variables for jets which attain supersonic velocity.

In any supersonic jet the flow at a certain distance downstream of the nozzle exit becomes subsonic ultimately. Consider a plane which divides the jet into two regions, namely, a region of mixed supersonic and subsonic flow upstream and a region of completely subsonic flow downstream. The upstream region, hereinafter referred to as the region of supersonic flow, will contain in any practical situation a pattern of shock and expansion waves which results in a transition to subsonic flow. The downstream region, hereinafter referred to as the subsonic region, has been shown for the case of a fully expanded jet (ref. 6)

to possess mean-flow characteristics, such as the mean-velocity profile, similar to those for a completely subsonic jet. Assume for present purposes that this is also sufficiently true for overexpanded and underexpanded jets. Also, assume that the fluctuating aerodynamic components in the subsonic region downstream behave similarly to those in a subsonic jet. (A small amount of experimental evidence (ref. 7) indicates that this assumption may be reasonably valid.) Then, the total-acoustic-power output of the jet can be expressed as the sum of the power contributions from the region upstream—containing supersonic flow—and the subsonic region downstream. The contribution from the subsonic region can be expressed in terms of the Lighthill parameter as $K\rho_0 A1^* a^{*8}/a_0^5$ (or $K\rho_0 A a_0^3$ for moderately choked jets having near-ambient temperatures), where A^* is the cross-sectional area of the jet at an effective sonic plane separating the upstream (supersonic flow) and downstream (subsonic flow) regions, and a^* is the critical speed of sound at this plane. The power contribution from the upstream region may originate from a variety of causes. One of these the interaction of turbulence and shock waves, has been studied theoretically by Ribner (ref. 8), who found that pressure fluctuations of considerable magnitude should result in the near field from the passage of turbulence through a shock wave. This source of noise may dominate in the supersonic region of jets containing strong shock waves, whereas aerodynamic noise sources may dominate throughout fully expanded jets. Assume, for the present, that shock-turbulence interaction is the principal source of noise in the upstream region, and consider the near-field relation between acoustic and flow variables found by Ribner (ref. 8, eq. (62)); effectively,

$$\overline{p'^2}(\xi-\xi_0 \leqq \lambda) \propto \frac{\overline{u'^2}}{a^{*2}} p^2 \tag{6}$$

where p is the mean static pressure at distance $\xi-\xi_0$ downstream of the shock. From the data in reference 9, it is apparent that the total power W_t is a function of the nozzle-exit area A also. This evidence indicates those variables which might be expected to affect the acoustic-power output from the region containing shock waves. From dimensional considerations it is shown in appendix B that this power contribution might be expressed as

$$W_c = \frac{p_0^2 A1}{\rho_0 a_0} g(P/p_0) \tag{7}$$

where $g(P/p_0)=0$ for $P/p_0 \leqq 1.89$. Combining the power contributions from the subsonic and supersonic regions results in

$$W_t = KL^* + \frac{p_0^2 A1}{\rho_0 a_0} g(P/p_0) \tag{8a}$$

or

$$g(P/p_0) = \frac{\rho_0 a_0}{p_0^2 A1} (W_t - KL^*) \tag{8b}$$

where L^* is associated with A^* and a^*, rather than with A and U. Equation (8b) is the form for determining g from experimental data, and equation (8a) is the form for computing the total power W_t for other conditions after g has once been determined.

Equation (8a), in conjunction with test data, might be used to estimate the relative magnitudes of the acoustic-power contributions from the upstream and downstream regions.

POWER SPECTRUM

The distribution of the total acoustic power as a function of frequency is referred to as the power spectrum. If $w(f)$ represents the acoustic power radiated in a frequency-bandwidth df at frequency f cycles per second, then

$$\frac{1}{W}\int_0^\infty w(f)\,df = 1 \tag{9}$$

A dimensionless-frequency form is given by fl/U, the Strouhal number. In terms of Strouhal number, equation (9) becomes, for nozzles having circular cross sections,

$$\int_0^\infty \left[\frac{U}{D}\frac{w(f)}{W}\right]\frac{D}{U}\,df = 1 \tag{10}$$

so that a dimensionless form of the power spectrum is given by $\frac{U}{D}\frac{w(f)}{W}$ as a function of the Strouhal number. Equation (10) applies for any flow condition. However, the functional relation between

acoustic power and the flow characteristics differs for subsonic and supersonic jets. This may be readily indicated by rewriting equation (10) in terms of the geometric and aerodynamic variables. Thus, for subsonic jets,

$$\int_0^\infty \left[\frac{4a_0^5 w(f)}{\pi K \rho_0 D^2 U^7}\right]\frac{D}{U}\,df=1 \tag{11}$$

by virtue of equation (5), whereas for supersonic jets a possible form (assuming eq. (8a) is confirmed by experiment) is

$$\frac{1}{W}\left\{\int_0^\infty \left[\frac{a^* w(f)}{D^*}\right]\frac{D^*}{a^*}\,df + \int_0^\infty \left[\frac{a w_c(f)}{D}\right]\frac{D}{a}\,df\right\}=1 \tag{12}$$

the derivation of which is outlined in appendix B. By applying equations (5), (7), and (8a), equation (12) could be readily expressed in a form equivalent to that of equation (11), if desired.

In reference 2 (figs. 45(a) and 45(b)), power spectra were correlated in a form equivalent to that corresponding to equation (10). In reference 10 (fig. 4) power spectra were correlated in a form essentially equivalent to that corresponding to equation (11), namely, $PWL - 10 \log D^3$ as a function of $f'D$ for denoted values of nozzle pressure ratio P/p_0. However, it is evident from equation (11) that the correlation in reference 10 is only valid for constant jet temperature. It is noteworthy that, in figure 4 of reference 10, good correlation of power spectra is shown for supercritical pressure ratios. However, the correlating parameters are based on the formula (11), which applies for subsonic jets.

DIRECTIVITY FACTOR

The total power and power spectrum represent integrated acoustic characteristics in that they describe the total radiation per second. At specific points in the noise field, the analogous quantities of interest are the acoustic intensity and the mean-square acoustic pressure (cf. eq. (3)) and their associated spectra. Of the two former quantities, only the mean-square acoustic pressure will be considered because it is most easily measured. However, the corresponding expressions for intensity can easily be derived (cf. appendix B).

The local mean-square pressure in the far field is given by

$$\overline{p'^2}(\vec{z})=k'(\theta)\,\frac{\rho_0 a_0 W}{4\pi r^2} \tag{13}$$

where the directivity factor $k'(\theta)$ is defined by

$$k'(\theta)=I(\vec{z})/\langle I(r)\rangle$$

and the field point $\vec{z}$ lies on the large sphere of radius r centered at the noise source (cf. fig. 1). Equation (13) is general. For subsonic jets,

$$\overline{p'^2}(\vec{z})=k'(\theta)K\,\frac{\rho_{0^2}^2 A U^8}{4\pi r^2 a_0^4} \tag{14}$$

For supersonic jets the corresponding relation is

$$\overline{p'^2}(\vec{z})=k'(\theta)K\,\frac{\rho_{0^2}^2 A^* a^{*8}}{4\pi r^2 a_0^4}+k_c'(\theta)\,\frac{p_{0^2}^2 A}{4\pi r^2}\,g(P/p_0) \tag{15a}$$

$$=k'(\theta)\left[K\frac{\rho_{0^2}^2 A^* a^{*8}}{4\pi r^2 a_0^4}+\alpha(\theta)\,\frac{p_{0^2}^2 A}{4\pi r^2}\,g(P/p_0)\right] \tag{15b}$$

Equations (15a) and (15b) represent alternative forms. In equation (15a), k_c' represents the directivity factor associated with the noise from the supersonic region. In equation (15b), $\alpha(\theta)=k_c'(\theta)/k'(\theta)$ is a directivity correction factor which accounts for the difference between the directivity patterns for subsonic and supersonic jets. Equations (13) to (15) are derived in appendix B.

The directivity factor $k'(\theta)$ is the linear equivalent of the directivity index used in reference 2. The directivity index, although not specifically defined as such, has also been utilized in references 11 and 1.

LOCAL PRESSURE SPECTRUM

The dimensionless expression for the local mean-square-pressure spectrum $\overline{p'^2}(f;\vec{z})$ is analogous to that for the power spectrum. The dimensionless form is

$$\frac{1}{\overline{p'^2}(\vec{z})}\int_0^\infty \left[\frac{U}{D}\overline{p'^2}(f;\vec{z})\right]\frac{D}{U}\,df=1 \tag{16}$$

which is to be exhibited in the form $\dfrac{U}{D}\dfrac{\overline{p'^2}(f;\vec{z})}{\overline{p'^2}(\vec{z})}$ as a function of Strouhal number. Equation (16) can be rewritten in terms of the flow variables

using equation (14) (subsonic jets) or equation (15) (supersonic jets). The result is analogous to equation (11) or (12), respectively, for the power spectrum. In particular, for subsonic jets the result is

$$\int_0^\infty \left[\frac{16r^2a_0^4\overline{p'^2}(f;\vec{z})}{k'(\theta)K\rho_0^2I^2U^7}\right]\frac{D}{U}\,df=1 \tag{17}$$

The dimensionless pressure spectra should possess shapes which are independent of the magnitude of $\vec{z}$ for all frequencies for which $\vec{z}$ is in the far field. (Recall that the distance from the turbulent region to the far field is a function of frequency.) However, because $\overline{p'^2}(\vec{z})$ is a function of θ, $\overline{p'^2}(f;\vec{z})$ might also be a function of θ. Therefore, spectra obtained at different azimuths are not necessarily similar.

The preceding formulas should be sufficient to permit prediction of the acoustic power, power spectrum, local acoustic pressures, and local acoustic-pressure spectra associated with the acoustic far field of all dynamically similar jets if the quantities K, $w(f)$, $k'(\theta)$, and $\overline{p'^2}(f;\vec{z})$, respectively, are determined experimentally for one jet.

PRESSURE PROBABILITY-DENSITY

The total acoustic power and local mean-square acoustic pressures symbolize the variance of the far-field pressures about the quiescent, or mean, value. The power spectrum and local pressure spectra are respective measures of the distribution of this variance with respect to frequency. Another independent quantity, the probability-density, or frequency function Φ', which has received relatively little attention in jet noise research, describes the distribution of local acoustic pressures with respect to probability of occurrence. (Of course, probability-density can be defined for any suitable variable.) Thus,

$$\text{Probability } (p_1'<p'<p_2')=\int_{p_1'}^{p_2'}\Phi'(p')\,dp' \tag{18}$$

where

$$\Phi'(p')=\frac{d\Phi}{dp'}$$

and

$$\int_{-\infty}^{\infty}\Phi'(p')\,dp'=1$$

(cf. ref. 12). The measured probability-density $\Phi'(p')$ may be related to the normal, or Gaussian, function

$$\varphi(p')=\frac{1}{\sqrt{2\pi}\sigma}e^{-\frac{1}{2}\left(\frac{p'}{\sigma}\right)^2} \tag{19}$$

by means of the Edgeworth series

$$\Phi'(p')=\varphi(p')-\frac{1}{3!}\frac{\mu_3}{\sigma^3}\varphi^{(3)}(p')+\frac{1}{4!}\left(\frac{\mu_4}{\sigma^4}-3\right)\varphi^{(4)}(p')$$
$$+\ldots=\varphi(p')\left[1+\frac{1}{3!}\frac{\mu_3}{\sigma^3}\frac{p'^3}{\sigma^6}+\frac{1}{4!}\left(\frac{\mu_4}{\sigma^4}-3\right)\frac{p'^4}{\sigma^8}+\ldots\right] \tag{20}$$

where

$$\mu_3=\int_{-\infty}^{\infty}p'^3\Phi'(p')\,dp' \tag{21}$$

$$\mu_4=\int_{-\infty}^{\infty}p'^4\Phi'(p')\,dp' \tag{22}$$

(cf. ref. 13). A measure of the closeness of the measured probability-density function to the normal function is obtained by computing the moments μ_3/σ^3, the coefficient of skewness, and $(\mu_4/\sigma^4)-3$, the coefficient of excess (or flatness).

APPARATUS

AIR-JET FACILITY

A diagram of the air-jet installation and a photograph of the downstream portion of the installation are shown in figure 2. In most respects, the air-jet system is similar to that described in reference 9. However, the preheater system shown in figure 2(a) was not utilized in the present test series. Air is supplied by remote compressors at a gage pressure somewhat less than 125 pounds per square inch and at near-ambient temperature. The plenum pressure is controllable. The jet emerges in a horizontal direction 10 feet above the ground plane and more than 100 feet from the nearest structure other than the jet installation itself. Three circular convergent nozzles (fig. 3), one having an exit diameter of 5 inches, the other two having exit diameters of 3 inches, were used. Tests on the two 3-inch-diameter nozzles were widely separated in time. (The acoustic absorbing material covering the plenum face and nozzle (fig. 2(b)) was removed before making far-field measurements. Also, the microphone actuator shown in the figure was removed during the present tests.)

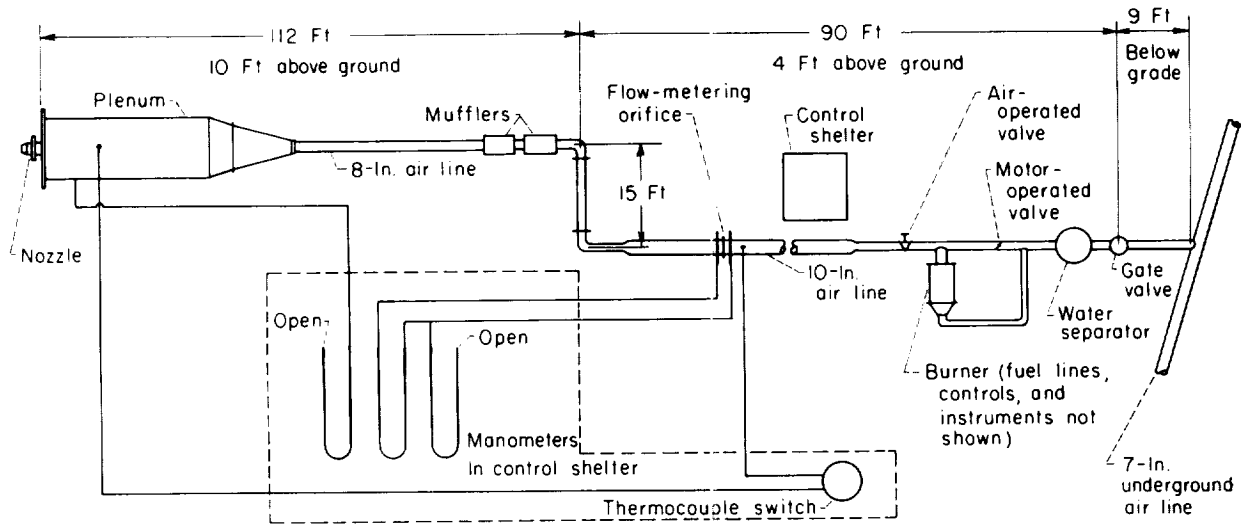

(a) Plan view (not to scale).

FIGURE 2.—Air-jet installation.

(b)

(b) Downstream portion.

FIGURE 2.—Concluded. Air-jet installation.

To determine the jet velocity, weight-flow rate of air, and nozzle discharge coefficient, a calibrated orifice plate was inserted in the air line at the point shown in figure 2(a). The following pressure differences were measured and indicated by mercury or water manometers:

(1) gage static pressure upstream of the orifice (mercury)
(2) static-pressure drop across orifice (water)
(3) gage static pressure in plenum (mercury).

Ambient pressure and temperature data were obtained from the United States Weather Bureau facility nearby. Temperatures were measured using iron-constantan thermocouples located upstream of the orifice plate and in the plenum. The computed nozzle pressure ratio was the static-pressure ratio. However, because the air velocity in the plenum was negligible, this ratio was equivalent to the ratio of the ambient static pressure to the plenum stagnation pressure.

ACOUSTIC RECORDING AND ANALYSIS

Acoustic data were recorded from a battery of essentially nondirective condenser microphones (as many as 11 microphones) mounted 10 feet

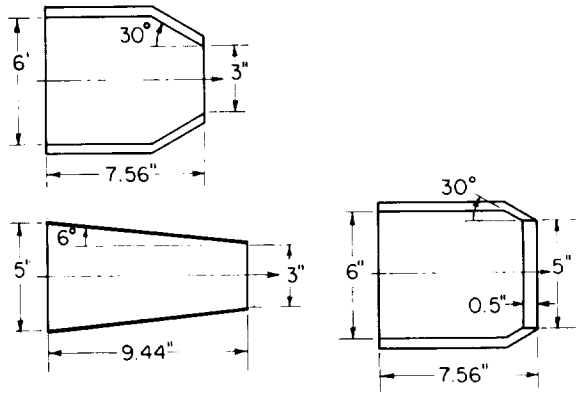

FIGURE 3.—Nozzle configurations.

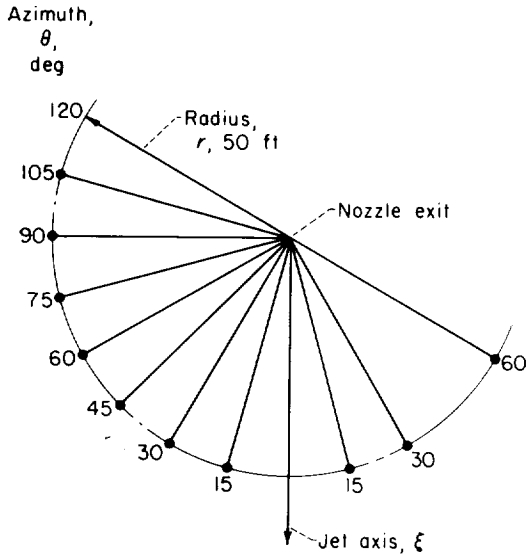

FIGURE 4.—Microphone stations.

above the ground plane on poles and located 50 feet from the nozzle exit at azimuth increments of 15°, as shown in figure 4. A block diagram of the acoustic-recording circuit is shown in figure 5. Microphone power supplies having very low impedance outputs permitted the use of long cables from the power supplies to the control room without introducing appreciable frequency distortion. At the control room, amplification of the signal in decade steps was provided in order to obtain an optimum input-signal amplitude for magnetic-tape recordings using a twin-channel recorder. A typical system-frequency-response curve (from microphone input through playback) is shown in figure 6. The microphone response

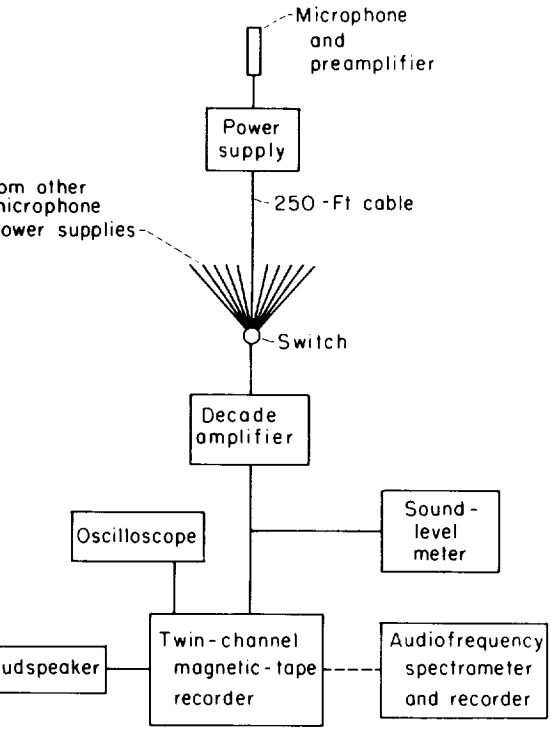

FIGURE 5.—Block diagram of acoustic recording and analyzing equipment.

532585—60——2

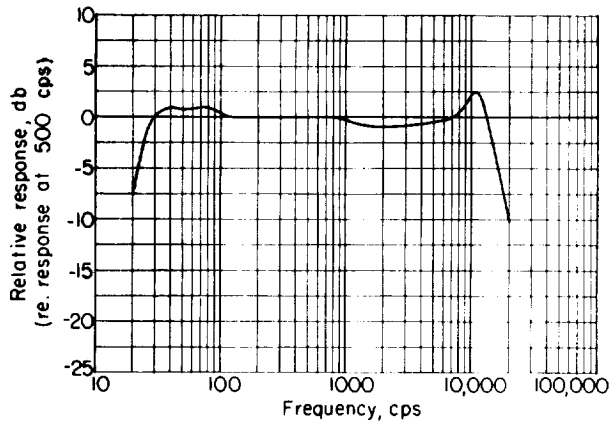

FIGURE 6.—Average response of complete acoustic systems (microphone inputs through playback). Record level, —10 voice units; tape speed, 15 inches per second.

accounted for most of the deviation from flat system-response. Each system was operated only within its range of linear amplitude-response. Signals were monitored at the output of the decade amplifier by a sound-level meter and at the output of one of the tape-recorder channels by an oscilloscope and a loudspeaker. Periodic calibrations at a single frequency were made using a miniature loudspeaker and a battery-operated oscillator.

Over-all sound-pressure levels were represented by the monitored levels. Noise spectra were transcribed from the tape recordings by means of a one-third-octave spectrum analyzer and an automatic level-recorder. The sound-level meter was a full-wave-rectified-averaging type, whereas the automatic level-recorder was a quasi-peak-averaging type.

Acoustic-pressure probability-densities were determined from the tape recordings by means of the probability analyzer described in reference 14.

PROCEDURE

The entire air-jet installation was shielded somewhat from the wind by distant buildings. However, as noted previously, wind data were obtained from the Weather Bureau facility nearby. Noise surveys were performed only when reported wind velocities were less than 20 miles per hour.

Preceding and following each series of tests a microphone calibration signal of known level (121 db re. 2×10^{-4} dyne/cm^2 at 400 cps) was monitored using the sound-level meter (cf. fig. 5). The signal waveform was monitored at the tape-recorder output to ensure against appreciable waveform distortion.

Airflow was initiated and adjusted to the desired conditions, and then the noise at each station was tape recorded. Over-all noise levels were monitored from the sound-level meter and noted when the wind was a minimum.

Because of the wide range of noise levels encountered during a single set of measurements, it was found desirable to adjust the recording level after establishing the selected flow conditions in order to ensure that recordings would remain within the range of linear system-response. The known calibration input-level and corresponding sound-level-meter reading plus the sound-level readings obtained while recording the noise were sufficient for determining noise levels. Acoustic power was calculated according to the method given in reference 15. Noise surveys were performed for several values of nozzle pressure ratio, both subcritical and supercritical.

RESULTS

TOTAL ACOUSTIC POWER

Subsonic jets.—The total acoustic power W radiated by subcritical flows from the 3- and 5-inch-diameter convergent nozzles is indicated in figure 7(a) as a function of the Lighthill parameter L. Both curves have slopes slightly greater than unity (on log graph paper), which indicates that the exponent of U is slightly greater than 8 (cf. ref. 5). The lateral displacement of the curves appears to result from the reduced value of the nozzle velocity coefficient C_v associated with the highly convergent nozzle (cf. appendix C). The total power output of the jet from the 3-inch-diameter, 30°-convergence-angle nozzle is approximately 2 decibels less than that from the less-convergent jets.

To al-acoustic-power determinations have also been reported in references 9 to 11 and 16 to 20. The various far-field noise characteristics considered in these reports are listed in table I. Additional data are contained in several unreferenced reports. However, these data are generally not sufficiently complete to permit the calculations indicated in this report. The 5-inch-diameter nozzle used in the present tests was identical to that reported on in reference 9. Otherwise, with the possible exception of certain of the engine tests reported in references 9 and 11, none of the nozzles were exactly similar. Moreover, as outlined in table II, experimental conditions were generally different. (For the largest values of the Lighthill parameter, the engine noise data, as well as the hot-jet noise data from ref. 20, are associated with choking of the jet, i.e., $P/p_0\approx 2.2$, and the flow is locally supersonic. However, these data fall along the total-power curve for subsonic jets. Therefore, jet-engine noise at rated engine speed will be discussed under the heading "Subsonic jets" throughout the remainder of this report. This similarity of hot choked jets to subsonic jets may result from a reduced effect of the shock pattern on noise generation from hot jets.)

The results of all tests are shown in figure 7(b). (Note that the data cover a range of nearly 100 lb. This corresponds to a power ratio of

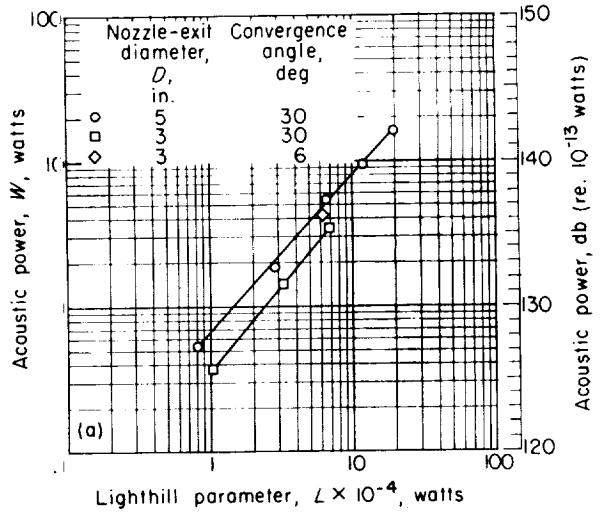

(a) Present tests.

FIGURE 7.—Total radiated acoustic power as function of Lighthill parameter.

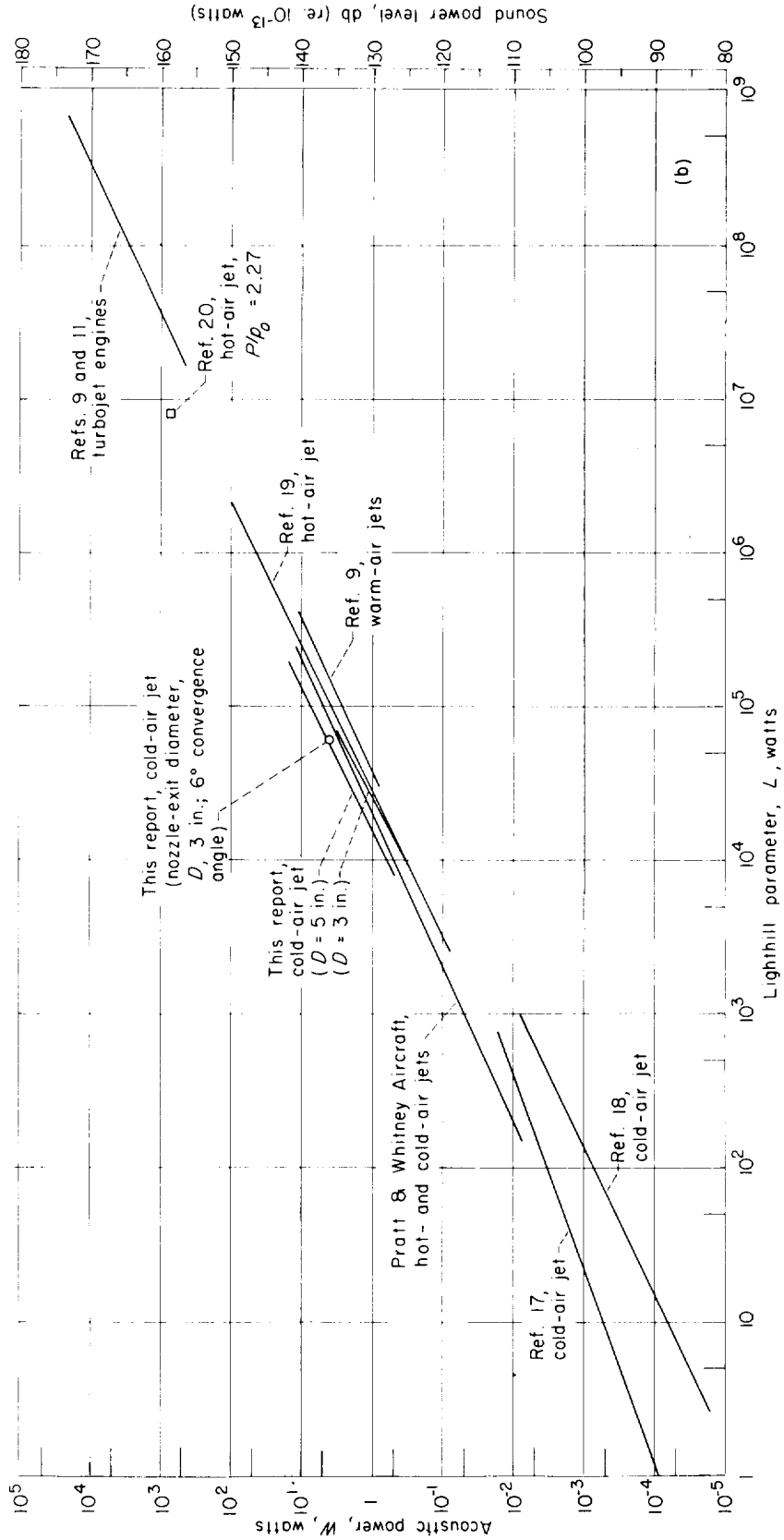

(b) All tests.

FIGURE 7. Concluded. Total radiated acoustic power as function of Lighthill parameter.

10^{10}, or a range of ten billion to one.) Most of the curves tend to satisfy equation (5). They spread over a range of W of nearly 5 decibels, except at the smallest values of L, where the spread is somewhat greater. The spread does not result from random errors of the individual data points (for which the scatter was generally less than 1 or 2 db), but rather results from systematic differences among the various experiments. (For example, the curve from Pratt & Whitney Aircraft data received in a private communication has L based on ρ, rather than ρ_0. On the basis of ρ_0, the slope of the curve would be slightly greater.) The acoustic-power curve from reference 16 is displaced so far from the trend of the curves in figure 7(b) that it was neglected.

The acoustic-power coefficient K can be determined by applying the appropriate equations in the section entitled ACOUSTIC SIMILARITY RELATIONS if mean-square acoustic pressures are measured in the far field in a quiescent, nonabsorbing, free space. Otherwise, correction of the data might be necessary. Factors to be considered in comparing the results of various experiments are listed in table II and discussed in appendix C. Estimated values of the significant corrections are listed in table III. However, no attempt has been made to correct the results shown in figure 7(b) because all possible significant errors, particularly the acoustic calibration error, could not be evaluated.

On the basis of the results shown in figure 7(b),

$$K \approx 3 \times 10^{-5}$$

According to Lighthill, large differences between the jet temperature and ambient temperature are likely to have only a small effect on the total acoustic power generated. From the curves shown in figure 7(b), no temperature effect is apparent (cf. ref. 19).

Supersonic jets.—Most of the available data on the acoustic-power output of supersonic jets is contained in references 2, 9, and 20. The data in reference 9 were correlated empirically in terms of W/A as a function of P/p_0, which was found to apply for subsonic as well as choked jets. When subsonic data for a wider range of jet temperatures are considered, the correlation fails. This should be expected (as pointed out in ref. 9), since $W/A = K\rho_0 U^8/a_0^5$ yields correlation. Correlation in terms of P/p_0 would require that P/p_0 be a unique function of $\rho_0 U^8/a_0^5$. This requirement is satisfied only for constant temperature.

In references 2 and 3 a correlation formula based on mechanical power of the jet is given. The formula obtained from rocket noise data is

$$PWL = 78 + 13.5 \log W_m \tag{17}$$

where PWL is in decibels (re. 10^{-13} watt), and the jetstream mechanical power W_m, in watts, is given by

$$W_m = FU_e \tag{18}$$

This formula fails to agree with the present results. However, in view of the wide divergence of the test conditions from which the formula was established with those of the present tests, the disagreement is not surprising.

The function $g(P/p_0)$ (cf. eq. (8b)) computed from the data in reference 9 and from the present tests is shown in figure 8 as a function of nozzle pressure ratio P/p_0. In computing g the assumptions were made that $A^* \approx A$ and $a^* \approx a$, so that the subsonic region downstream was regarded, from the standpoint of noise radiated, as equivalent to the same nozzle operated at critical pressure ratio and at the same exit temperature. No systematic cause of the spread of the cold jet data for convergent nozzles, other than geometric dissimilarity of the jets, is apparent. The repeat test results for the 3- and 5-inch-diameter nozzles are in good agreement with the original results from reference 9. The majority of the data is restricted to a narrow range of diameters and temperatures. For g expressed in terms of the plenum static pressure, rather than the ambient pressure p_0, the correlation was not nearly so good, as was expected.

One datum point (from ref. 20) in figure 8 (cf. fig. 7(b) also) is associated with a hot jet. The extremely large value of g for this nozzle, as well as the fact that most of the noise from the convergent-divergent nozzle at design pressure ratio is attributed to shock-turbulence interaction (fig. 9), indicates that the significance of the interaction on noise production is probably greatly overrated by using equation (8a). Aerodynamic noise may dominate in the supersonic region as well as in the subsonic region.

It is important to note that the effect of large

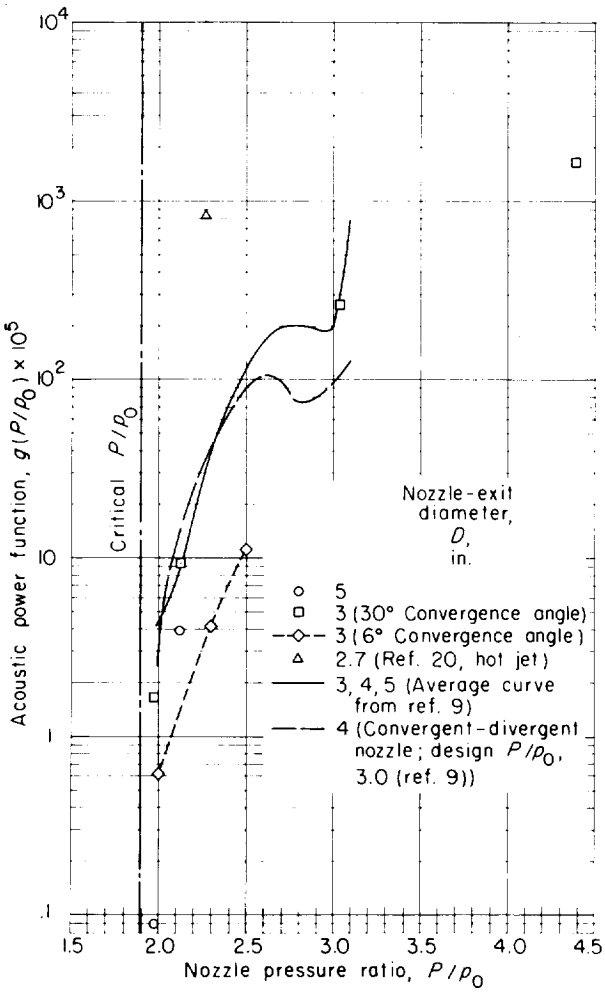

FIGURE 8.—Acoustic power function $g(P/p_0)$ as function of nozzle pressure ratio P/p_0.

changes of ambient conditions on total-power correlations has not been tested experimentally. This is also true for all the correlations which follow.

ACOUSTIC-POWER SPECTRUM

Subsonic jets.—Power spectra associated with subcritical flows from the 3- and 5-inch-diameter nozzles are shown in the appropriate dimensionless form (cf. eqs. (10) and (11)) in figure 10. The spectra for the smaller diameter nozzle are somewhat more peaked. This results from geometric dissimilarity of the nozzles and is not an effect of Reynolds number or Mach number. Corresponding spectra from previously published data are presented in figure 11. The spectra are generally similar except at the low-frequency end. Scatter of the spectra at the low-frequency end is caused by pseudosound resulting from wind impingement on the microphone. This masks possible near-field effects which may be present at the lower acoustic frequencies (cf. ref. 21). This low-frequency portion of each spectrum is neglected, and the bounds of the assemblage are shown in figure 12. No average curve is drawn. Additional data might only be expected to fall within the bounds shown. In figure 12(a) the spectrum for the larger air jets ($D>2$ in.) and turbojet engines is shown. The spread of the data is roughly 10 decibels, except at the highest audio-frequencies, where the spread is nearly 20 decibels. Part of the spread of the extreme bounds of the spectrum at the high-frequency end likely results from failure in a few of the experiments to correct measured spectra for instrumental deviations from flat frequency-response. However, slight differences of the lip configuration of the various nozzles may also influence the spectra at high frequencies because the high-frequency noise is

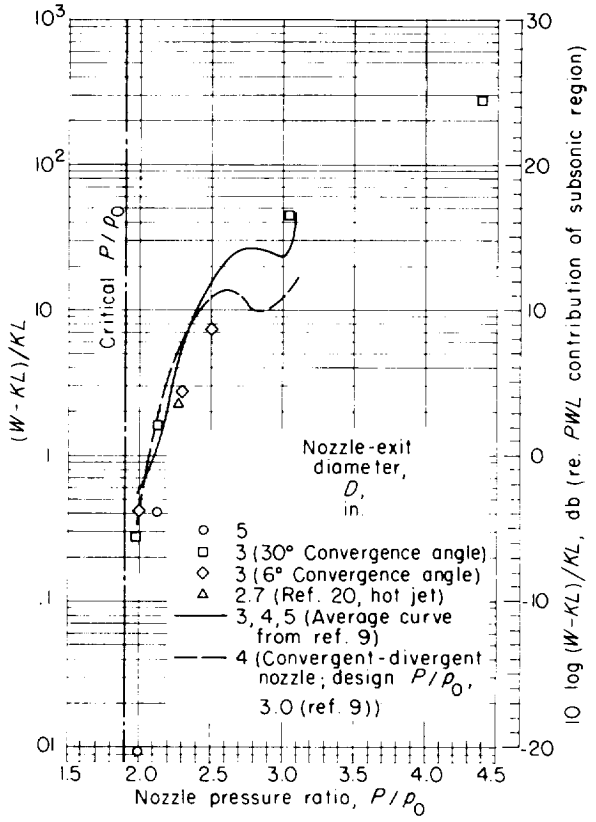

FIGURE 9.—Ratio of acoustic power contribution from supersonic region upstream to that from subsonic region downstream as function of nozzle pressure ratio P/p_0.

generated primarily near the lip. The collective spectrum for small air jets ($D<2$ in.) is shown in figure 12(b). It differs significantly from that of the larger jets in that the spectrum slope is lesser at the lower frequencies and greater at the higher frequencies. The spectra from references 16 and 17 are exceptions to this rule, however.

The dimensionless power-spectral-density curves are generally quasi-symmetric on the logarithmic plot and tend to peak in the interval $0.1 \leqq f'\frac{D}{U} \leqq 0.2$ for which $0.6 \leqq \frac{U}{D}\frac{w(f')}{W} \leqq 5$. The fall-off rate is slightly greater on the high-frequency end of the spectrum than on the low-frequency end.

The spectra in figure 11(f) show a slightly increased fall-off rate on the high-frequency end and a reduction of the Strouhal number of the spectrum peak as the jet temperature is increased. These data were taken indoors, hence were unaffected by wind, whereas the corresponding data in figure 11(e) were obtained outdoors. The change in spectrum shape appears compatible with the change in the jet velocity distribution, hence geometric dissimilarity, which occurs as the jet temperature is changed.

Supersonic jets.—Dimensionless spectra computed from the present data are shown in figure 13. The correlation is presented in terms of a, rather than U, because of choking. The spectra tend to peak in the interval $1 \leqq \frac{a}{D}\frac{w(f')}{W} \leqq 3$; $0.1 \leqq f'\frac{D}{a} \leqq 0.2$, except where discrete-frequency whistles occur. These dimensionless spectra are generally in excellent agreement with the spectra for subsonic flow from the same nozzles (cf. fig. 10). The spectra for the 3-inch-diameter nozzle include discrete-frequency whistles. Near the whistle frequency the spectra do not correlate. The 5-inch-diameter nozzle did not produce whistles.

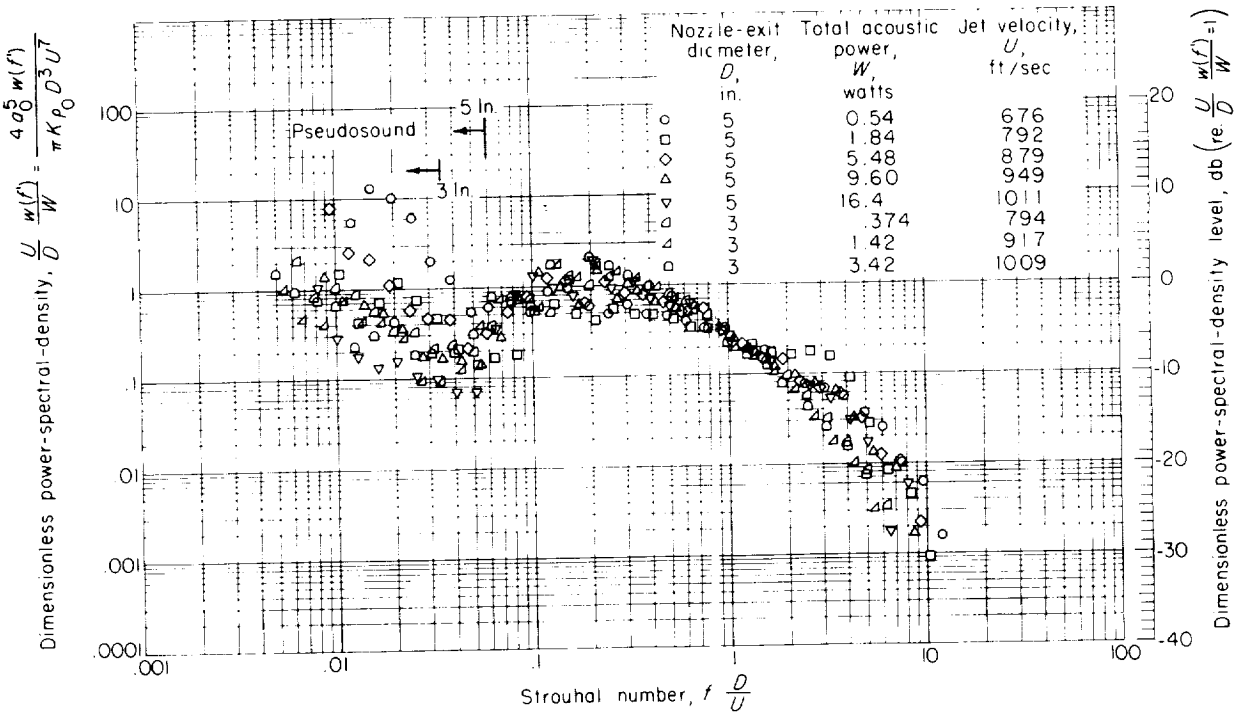

FIGURE 10. Dimensionless power-spectral-density functions for subsonic air jets. Present tests; ambient temperature, 522° R (approx.).

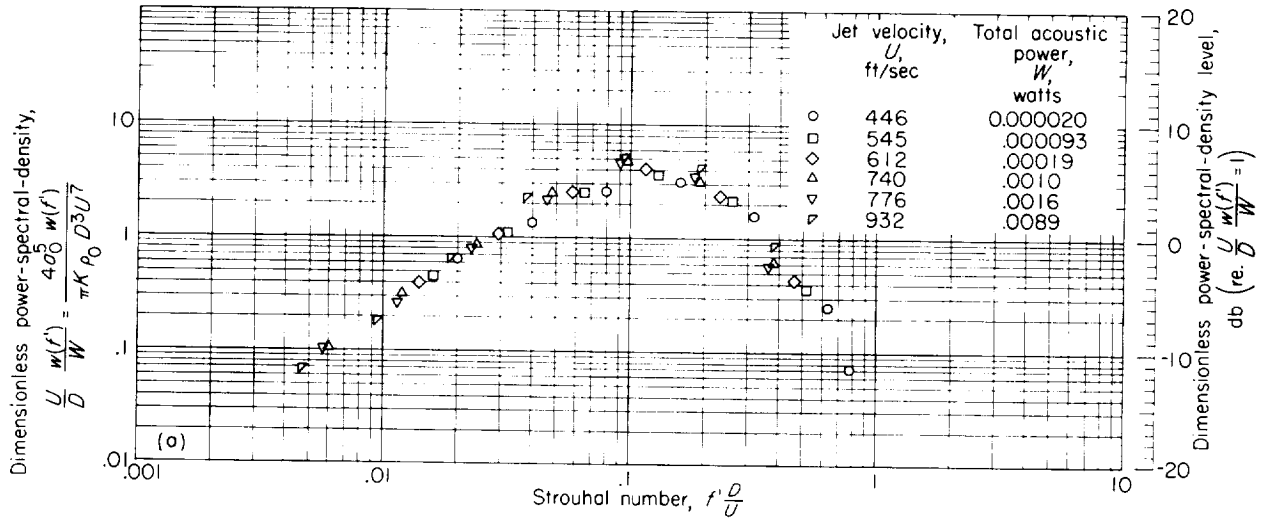

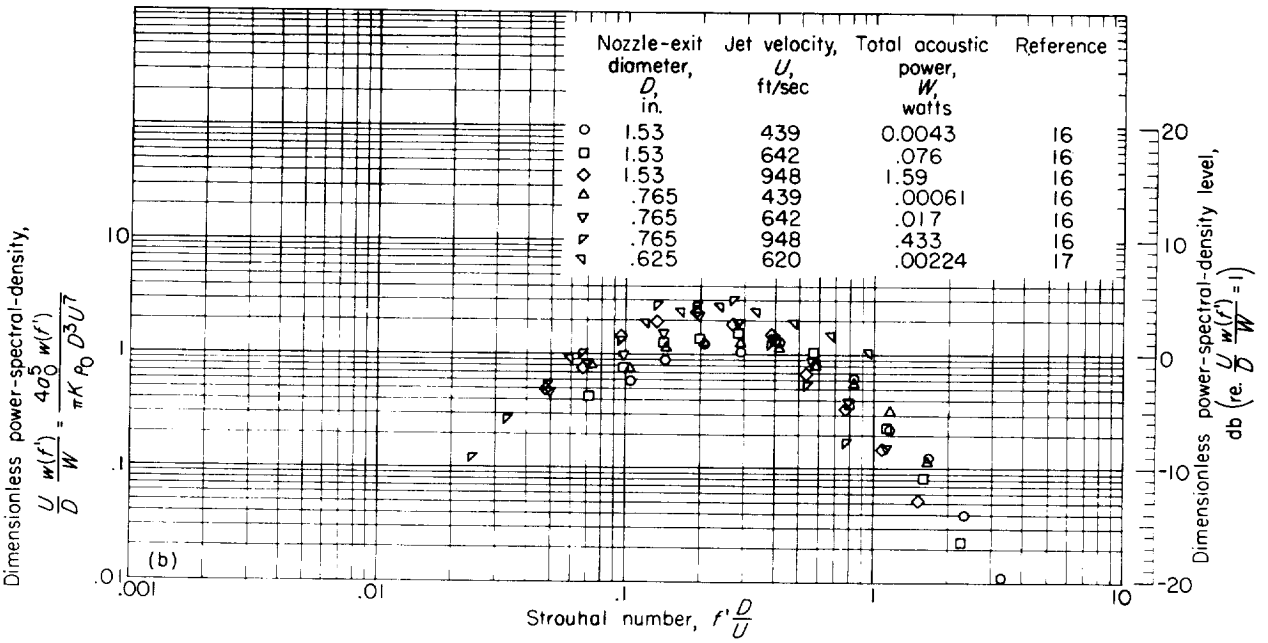

(a) Air jet (ref. 18). Nozzle-exit diameter, 0.5 inch; ambient temperature, 528° R.
(b) Air jets (refs. 16 and 17). Ambient temperature, 528° R (approx.).

FIGURE 11. –Dimensionless power-spectral-density functions for subsonic jets.

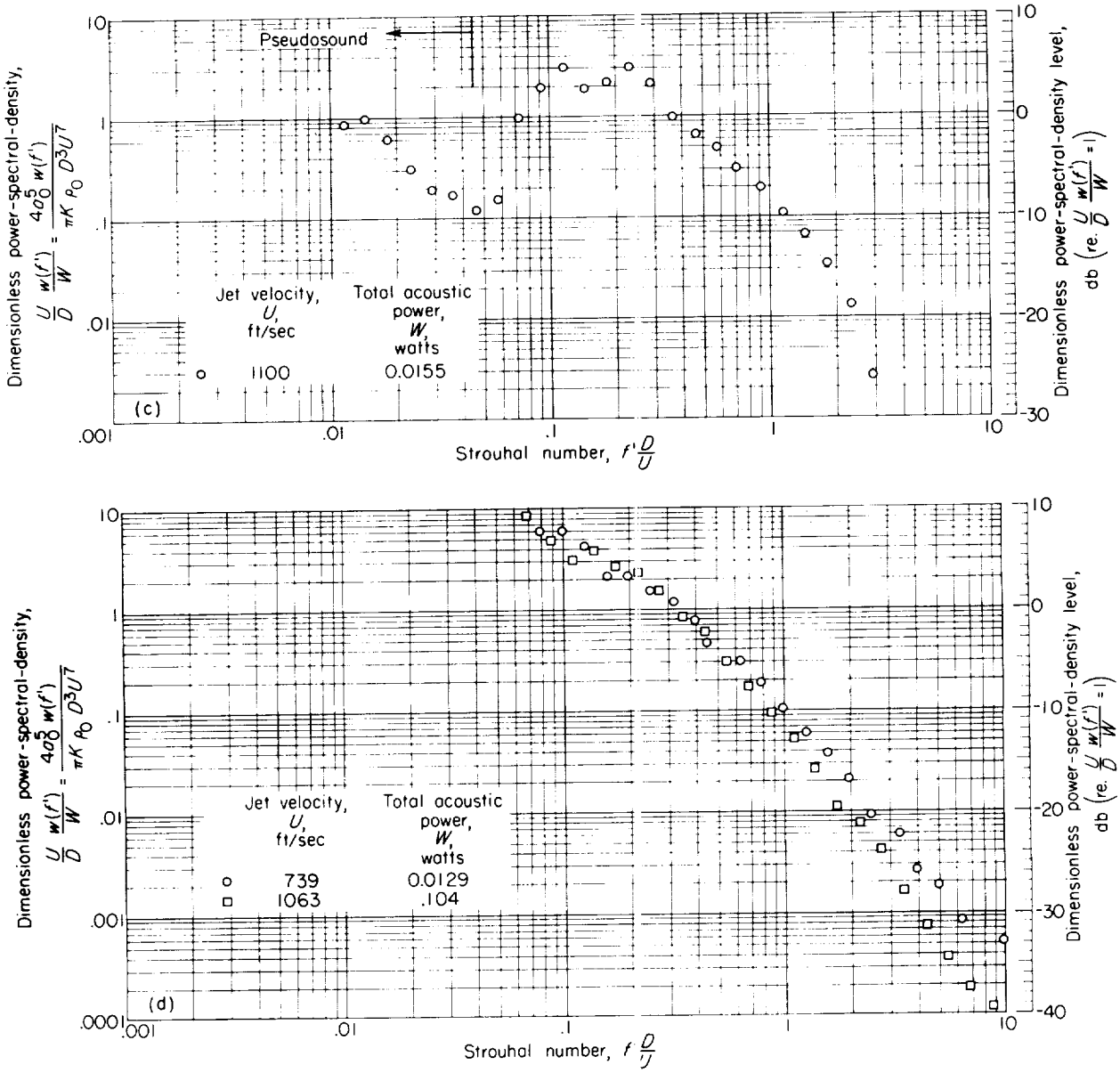

(c) Air jet (from fig. 14 of ref. 9). Nozzle-exit diameter, 4 inches; ambient temperature, 519° R.
(d) Air jet (from fig. 2 of ref. 10). Nozzle-exit diameter, 4 inches; ambient temperature, ?.

FIGURE 11.—Continued. Dimensionless power-spectral-density functions for subsonic jets.

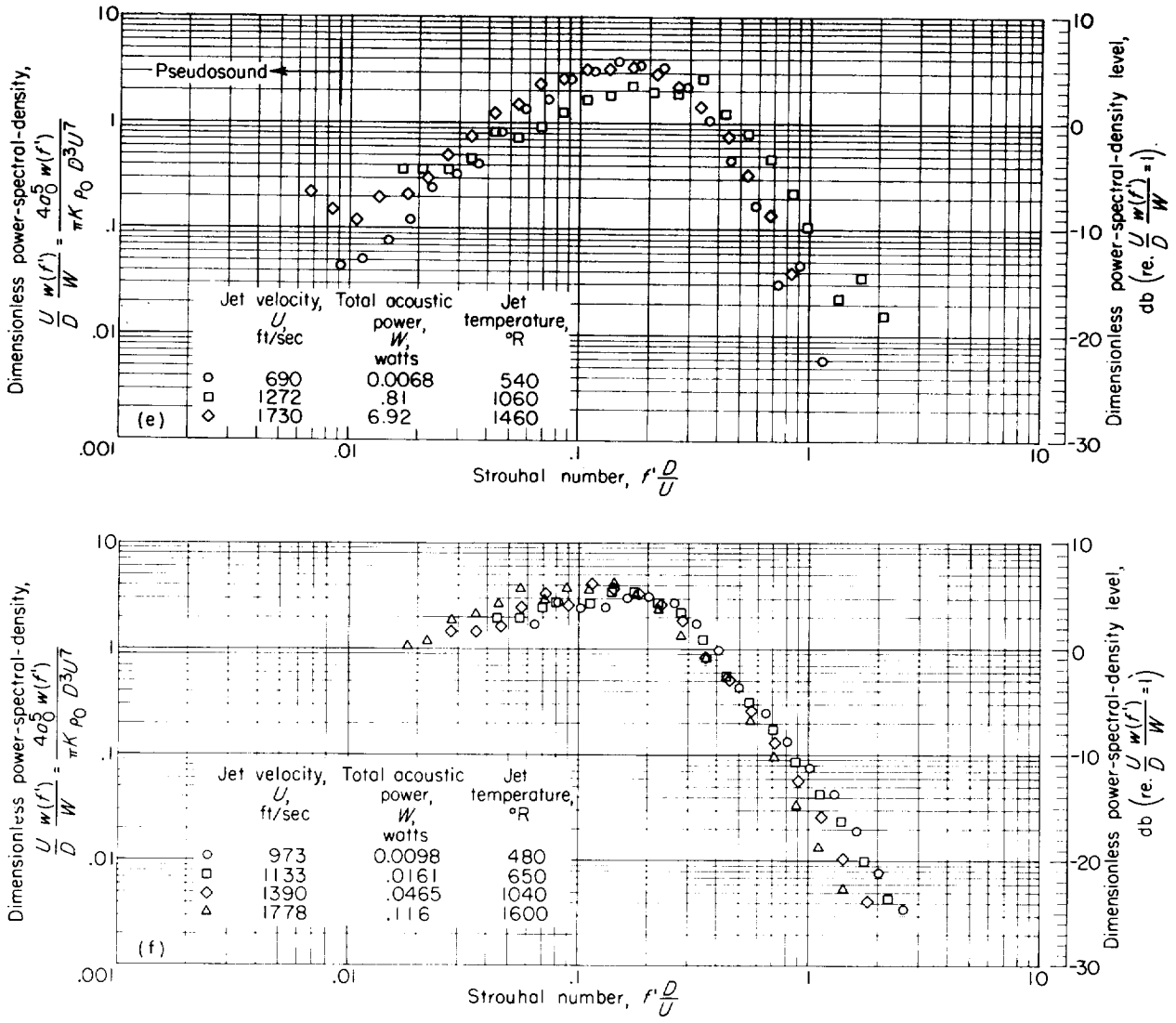

(e) Effect of air-jet temperature (ref. 19). Nozzle-exit diameter, 0.5625 inch; ambient temperature, 545° R (approx.).
(f) Effect of air-jet temperature (from fig. 16 of ref. 10). Nozzle-exit diameter, 1.9 inches; ambient temperature, ?.

FIGURE 11.—Continued. Dimensionless power-spectral-density functions for subsonic jets.

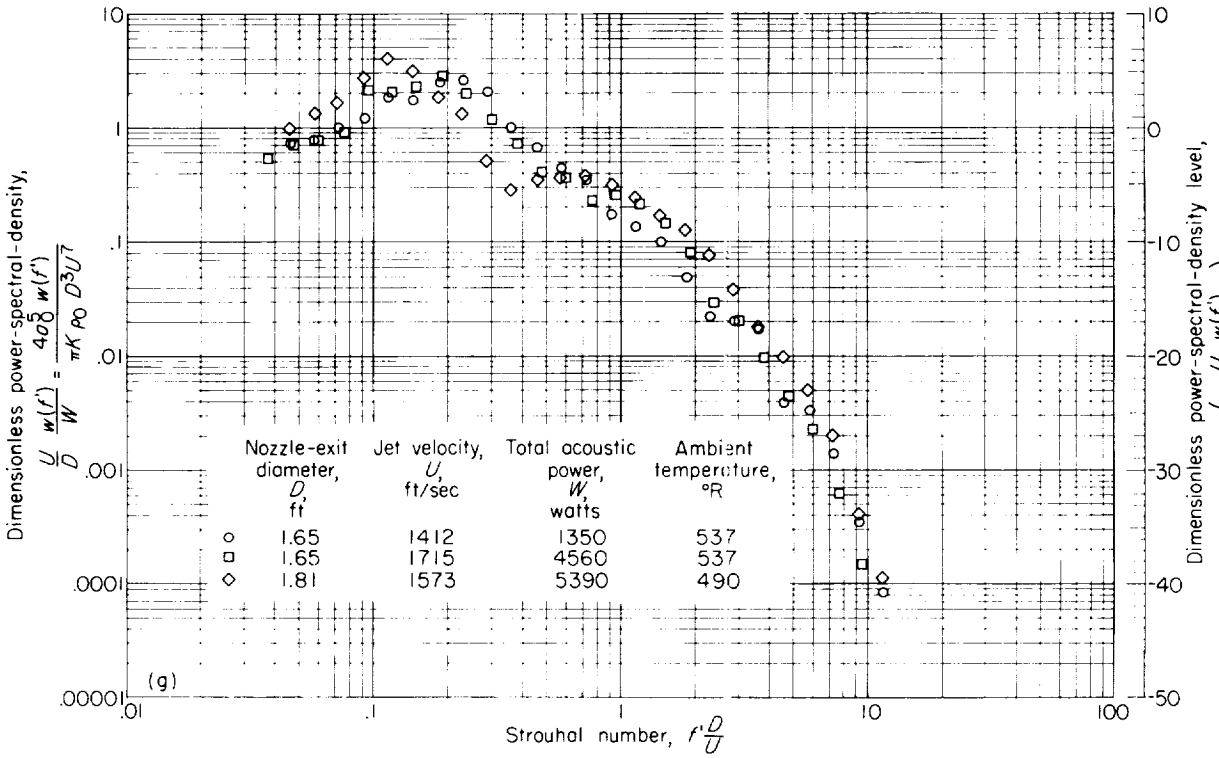

(g) Turbojet engines (from unpublished NACA data.)

FIGURE 11. Concluded. Dimensionless power-spectral-density functions for subsonic jets.

Spectra computed from previously published data are shown in figure 14. Spectra from any one experiment are in good agreement. However, there is some difference among the results from different experiments. All results, with the possible exception of those for model jets in figure 14(b), are for hot jets. Figure 14(b) (ref. 2, fig. 45B) shows an average curve for model jets, turbojet engines, and rockets. It is claimed in reference 2 that the data for all jets agree best when the comparison is based on a, but that the similarity of rocket data alone is best when based on U. This may result from the fact that the rocket nozzles were designed to minimize shock strengths. From the rocket data shown in reference 2, it appears that the value of Strouhal number (based on a) at which the spectrum peaked tended to be a slightly decreasing function of thrust. A similar result is shown in figure 14(a), where the effect is related to temperature.

For hot jets there is no evidence of whistling. In fact, the absence of whistling appears to be generally characteristic of hot jets. The effect of jet temperature is shown in figure 14(a) using data from reference 10. The result is similar to that for subsonic jets, namely, a reduction of the Strouhal number of the spectrum peak and an increased fall-off rate on the high-frequency end of the spectrum as temperature is increased.

ACOUSTIC-DIRECTIVITY FACTOR

Subsonic jets.—The directivity factor $k'(\theta)$ for the three nozzles and subsonic flow conditions is shown in figure 15 as a function of azimuth θ (cf. fig. 4 measured with the flow direction as the origin In all cases $k'(\theta)$ is a maximum ($k' \approx 3$) near $t = \pm 30°$.

Corresponding results for other tests are shown in figure 16. Directivity patterns were determinable only from data obtained in the "free field,' that is, outdoors. They are generally similar to the present results. The maximum value of $k'(\theta)$ is generally larger ($k'(\theta) \approx 6$) for the turbojet engines and occurs at an angle slightly greater than $\pm 30°$. This is regarded as a temperature effect. For large values of azimuth, that

is, upstream, noise from the engine inlet might be expected to yield larger values of $k'(\theta)$ than for air jets. At least for $\theta \leqq 120°$ (the limiting value of θ for the air-jet tests), no increase appears. The extreme increase of $k'(0)$ as a function of U shown in figure 16(a) likely resulted from jet impingement on the microphone.

The assemblage of patterns for subsonic jets, both hot and cold, is shown in figure 17.

Supersonic jets.—The directivity patterns, as determined from the present tests, are shown in figure 18. The maximum value of $k'(\theta)$ and its associated angle are approximately the same as for the subsonic case. The scatter of the data for the 3-inch-diameter nozzle at the large values of azimuth is probably induced by the discrete-frequency, and often unstable, whistling.

Other results are shown in figure 19. For a hot

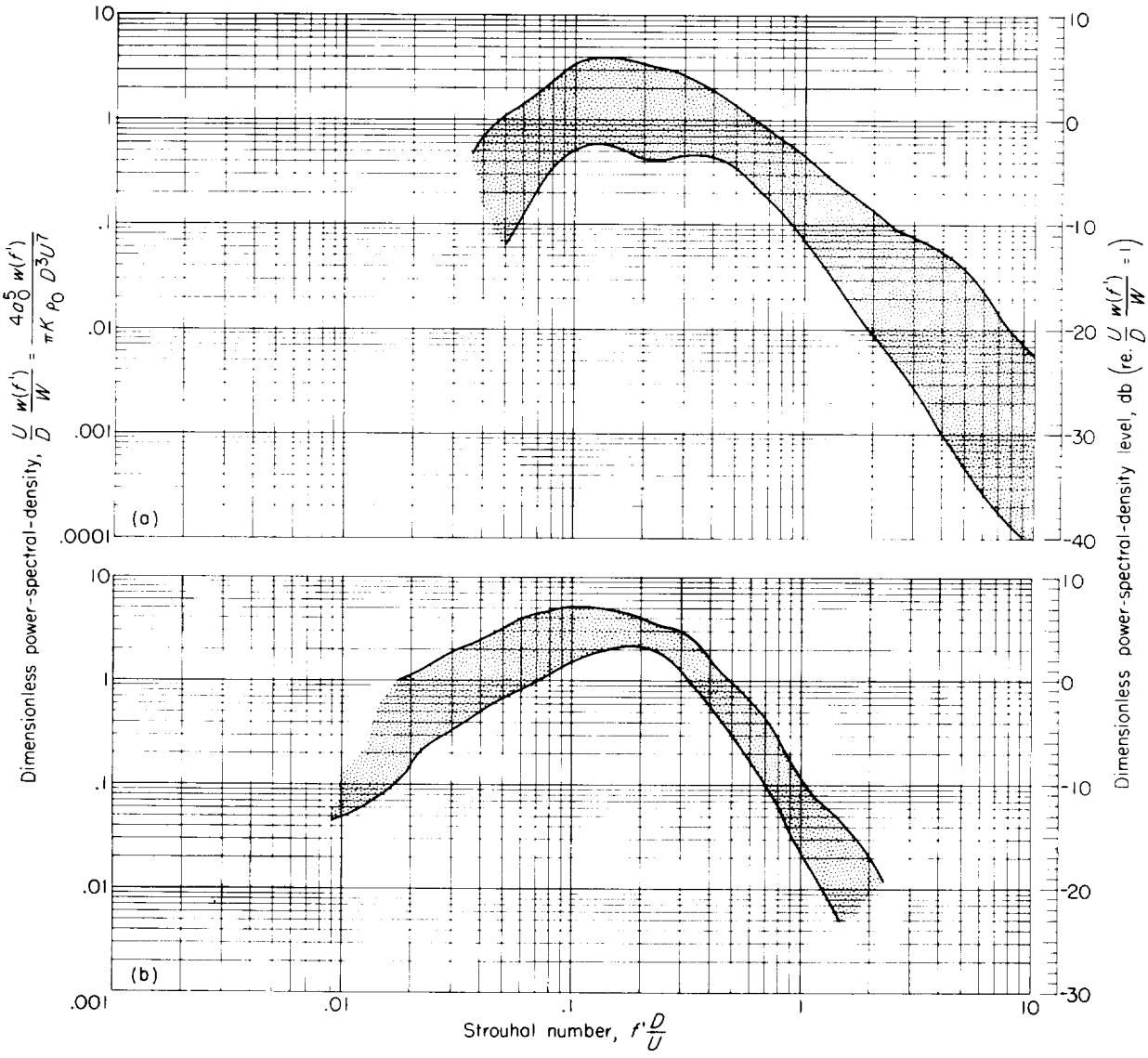

(a) Nozzle-exit diameter, >2 inches (refs. 9, 10, 16, 17, and present tests).
(b) Nozzle-exit diameter, <2 inches (refs. 10, 18, and 19).

FIGURE 12.—Collective power spectra for subsonic jets.

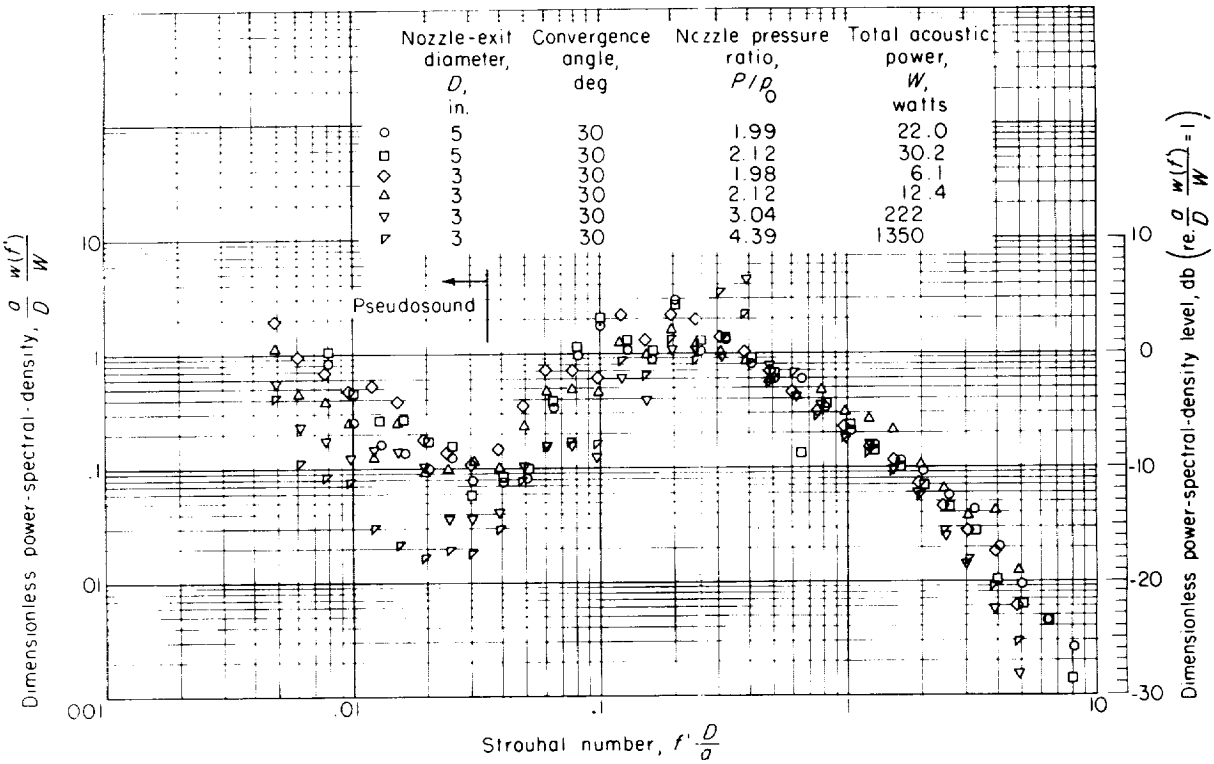

FIGURE 13. Dimensionless power-spectral-density functions for supersonic air jets. Present tests.

air jet (fig. 19(c)) the maximum value of $k'(\theta) \approx 7$ and occurs at a slightly larger value of azimuth. This larger value of $k'(\theta)$ for small θ is necessarily accompanied by a large reduction of $k'(\theta)$ in upstream directions (θ large).

Afterburning turbojet-engine directivity patterns are shown in figure 19(b). Here, the maximum value of $k'(\theta) \approx 5$ at $\theta \approx 45°$, that is, the angle of maximum propagation increases as the temperature is increased. This result is the same as in the subsonic case. The maximum value of $k'(\theta)$ may also increase. This is not assured, as shown in figure 19(d), which represents an average pattern for rockets from data in reference 2 (fig. 46). Here, at its maximum value, $k'(\theta) \approx 3$. However, for $k'(\theta)$ maximum, $\theta \approx 52°$, which again illustrates the increase of the angle of maximum propagation at high temperatures. Note that the rocket data are for convergent-divergent nozzles, so that the low value of maximum $k'(\theta)$ may be an effect of nozzle geometry.

LOCAL ACOUSTIC-PRESSURE SPECTRA

Subsonic jets.—Approximate—in that the meter-averaging characteristic was a rectified average—representations of dimensionless mean-square pressure-spectral-density at two values (30° and 90°) of azimuth are shown in figure 20 for the 3- and 5-inch-diameter nozzles. The spectra for the two nozzles at the same value of azimuth are in good agreement. The spectra for $\theta = 30°$ peak in the interval $1 \leqq \frac{l'}{D} \frac{\overline{p'^2}(f'; \vec{z})}{\overline{p'^2}} \leqq 3$; $0.1 \leqq f' \frac{D}{l'} \leqq 0.2$, which corresponds to the coordinates of the peak of the total-power spectrum, whereas the spectra at 90° attain a smaller peak value at a larger value of Strouhal number. Thus, the spectra at 30° are identical to the total-power spectrum, which partly confirms the known fact that the noise near 30° provides the dominant contribution to the power spectrum. The spectra are somewhat more peaked for the smaller diameter nozzle, as in the case of the power spectra, and at the smaller value of azimuth.

The scatter of the spectra at the lower frequencies is, of course, caused by wind.

Spectra for the 3-inch-diameter nozzle and a 4-inch-diameter convergent-divergent nozzle from data obtained at an earlier date are shown in fig-

ures 21(a) and (b). Except for their somewhat greater scatter, these results are in agreement with those from the present tests.

Turbojet-engine data for three values of azimuth are shown in figure 21(c). These spectra are not in good agreement with the air-jet spectra. There are at least four probable causes of the disagreement; namely, wind, ground reflections, jet temperature difference, and near-field effects. The corresponding power spectra are in much better agreement because of the smoothing effect of the integration process required to compute them.

Supersonic jets.—With the exception of effects of whistles (3-in.-diam. nozzle) and some increase in scatter, these spectra (fig. 22) agree fairly well and are also in good agreement with the corresponding subsonic results. Where the whistle is intense, a significant reduction of intensity occurs in frequency bands adjacent to that containing the whistle frequency (cf. fig. 22(a), $D=3$ in., $P/p_0=4.39$). Earlier tests (figs. 23(a) and (b)) of the 3-inch-diameter nozzle, except for having more scatter, are in agreement with the present results. As in the subsonic case, spectra for the turbojet engine do not agree with the air-jet spectra. The afterburning- and nonafterburning-engine results are in agreement for $\theta=90°$ but not for $\theta=45°$. The data are too limited to decide whether or not similarity actually exists. Ground reflection and near-field effects appear to be significant (cf. appendix C) by virtue of the oscillations of the spectra.

The dimensionless local-pressure spectra based on U and a are shown for a convergent-divergent nozzle in figures 24(a) and (b), respectively. The velocity range is so small that the correlations are equally good. The convergent-divergent-nozzle spectra possess the same correlation for subsonic and supersonic flow, just as do the spectra for convergent nozzles.

ACOUSTIC-PRESSURE PROBABILITY-DENSITY

Subsonic jets.—Acoustic-pressure probability-density-distributions for two values of azimuth (30° and 120°) are shown in figure 25. The normal function is also shown for comparison. Computed

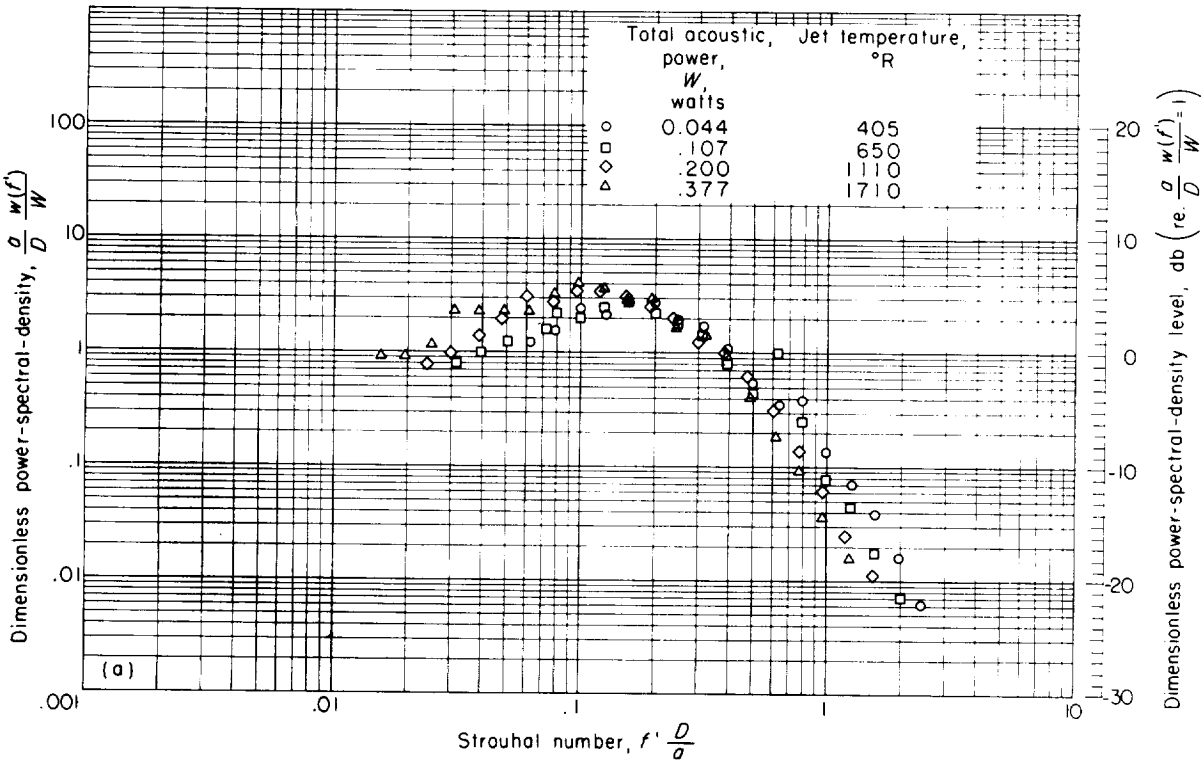

(a) Effect of air-jet temperature (from fig. 17 of ref. 10). Nozzle-exit diameter, 1.9 inches; nozzle pressure ratio P/p_0, 2.3.

FIGURE 14.—Dimensionless power-spectral-density functions for supersonic jets.

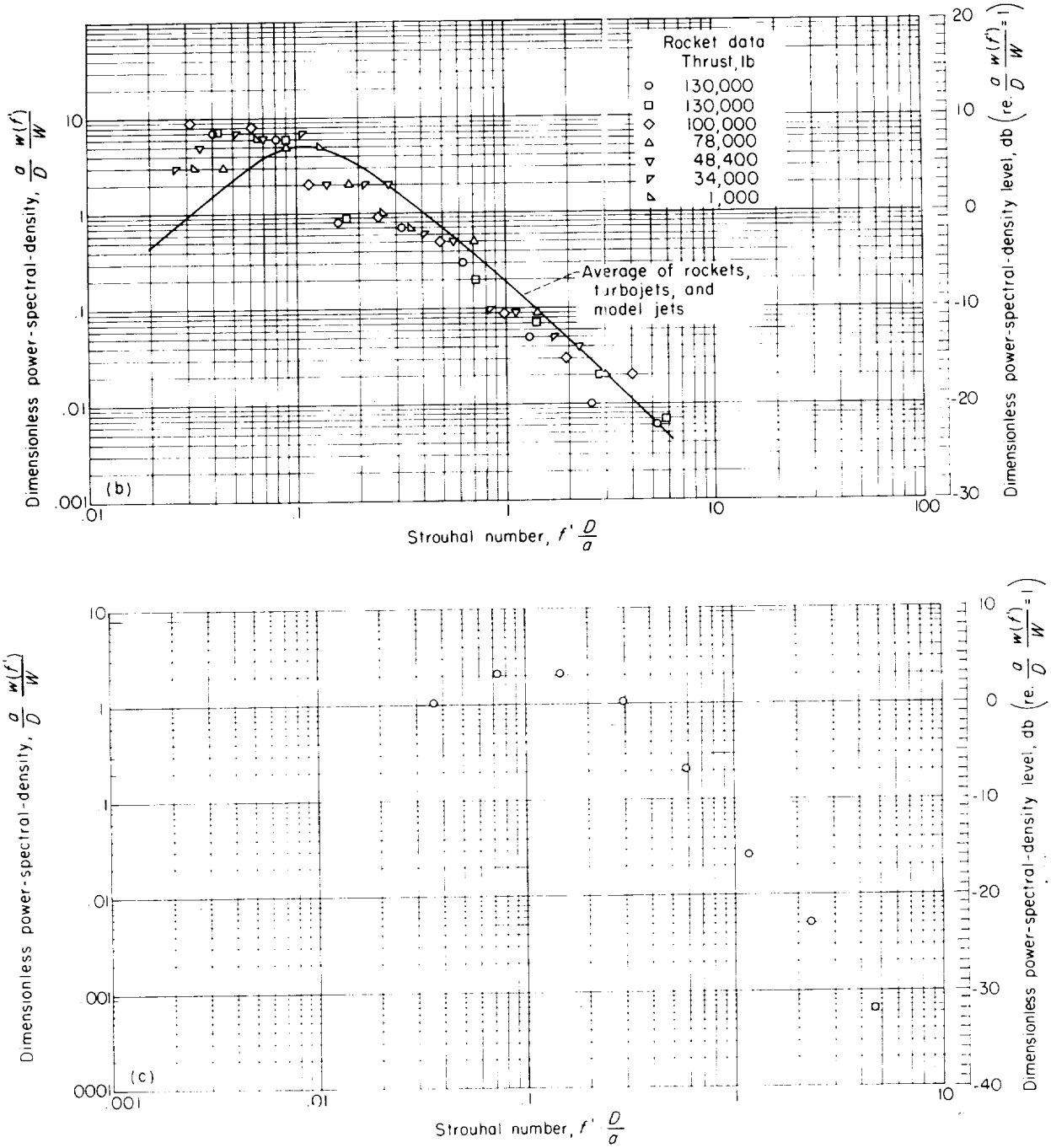

(b) Rockets with convergent-divergent nozzles, turbojet engines, and model jets (fig. 45B of ref. 2).
(c) Hot air jet (from fig. 9 of ref. 20). Nozzle-exit diameter, 2.7 inches; nozzle pressure ratio P/p_0, 2.27; total acoustic power, 798 watts; jet temperature, 1437° R.

FIGURE 14. Concluded. Dimensionless power-spectral-density functions for supersonic jets.

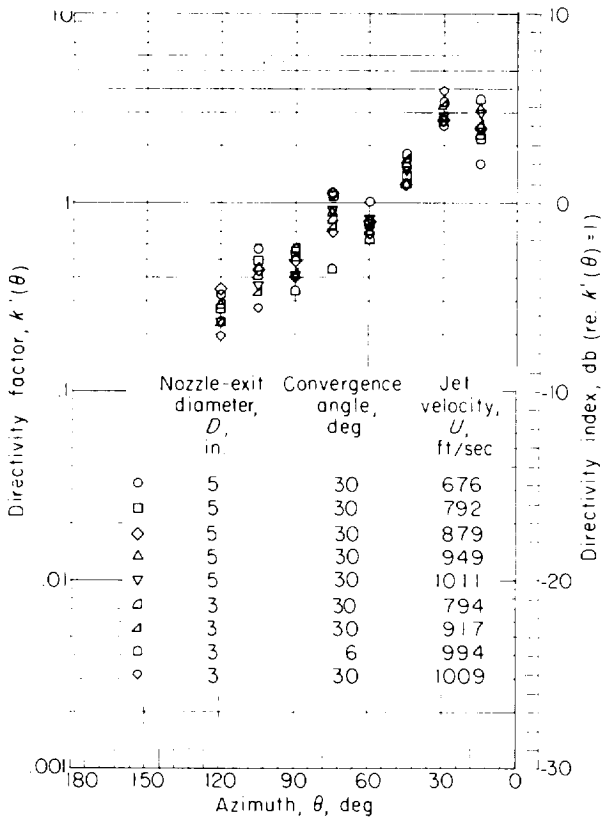

FIGURE 15.—Directivity functions for subsonic air jets. Present tests.

values of the skewness and flatness coefficients are listed in the following table:

D, in.	U, ft/sec	θ, deg	μ_3/σ^3	$(\mu_4/\sigma^4)-3$
5	879	30	−0.28	−0.016
5	879	120	−.56	−.43
3	917	30	−.28	−.37
3	917	120	.08	−.66

Although some deviation from the normal density-distribution is indicated, it does not appear to be great. From equation (20), this deviation from normality is most influential for the larger excursions of acoustic pressure. From the physical standpoint, a certain amount of deviation from normality should be expected simply because of the finite measuring time (of the order of 10 sec). For this reason also, the maximum excursion of the pressure is somewhat indeterminate (cf. ref. 22).

For both the 3- and 5-inch-diameter nozzles, the probability-density-distribution for $\theta=120°$ is less smooth and deviates by a greater amount from the normal curve than does the distribution for $\theta=30°$. This results from the smaller ratio of signal (jet noise) to noise (wind noise) at $\theta=120°$. The effect of wind appears to be considerable. The largest deviations of $\Phi'(p')$ from the normal curve were caused by wind impingement on the microphone. From the small number of results shown, it is estimated that $\mu_3/\sigma^3\approx 0.3$ and $(\mu_4/\sigma^4)-3\approx -0.3$ for all values of the variables considered. No sign has been attached to either the value of the skewness coefficient or to the pressure amplitudes in figure 25, because the relation between the sign of the voltage and pressure was practically indeterminate in the present experiment. The signs of the values of the skewness coefficient in the table are arbitrary with respect to the sign of the acoustic pressure.

Supersonic jets.—Probability-density-distributions associated with supersonic jets are shown in figure 26. Computed values of the skewness and flatness coefficients are as follows:

D, in.	a, ft/sec	P/p_0	θ, deg	μ_3/σ^3	$(\mu_4/\sigma^4)-3$
5	1030	0.470	30	−0.31	0.16
5	1030	.470	120	−.77	.03
3	1026	.472	30	−.34	.11
3	1026	.472	120	−.33	.34

At higher values of P/p_0, hence higher noise levels, wind effects are less significant. No appreciable systematic deviation from the normal curve as a function of azimuth is evident from figure 26. Computed values of the skewness coefficient are similar to those for the subsonic case, that is, $\mu_3/\sigma^3\approx 0.3$ (sign not determined).

The moments for the 3-inch-diameter nozzle include the effects of the discrete-frequency whistles. It may be concluded that the effect of the pressure contribution of the whistle is small compared to the effect of the contribution of the continuous spectrum because there is no systematic deviation of the values of the moments.

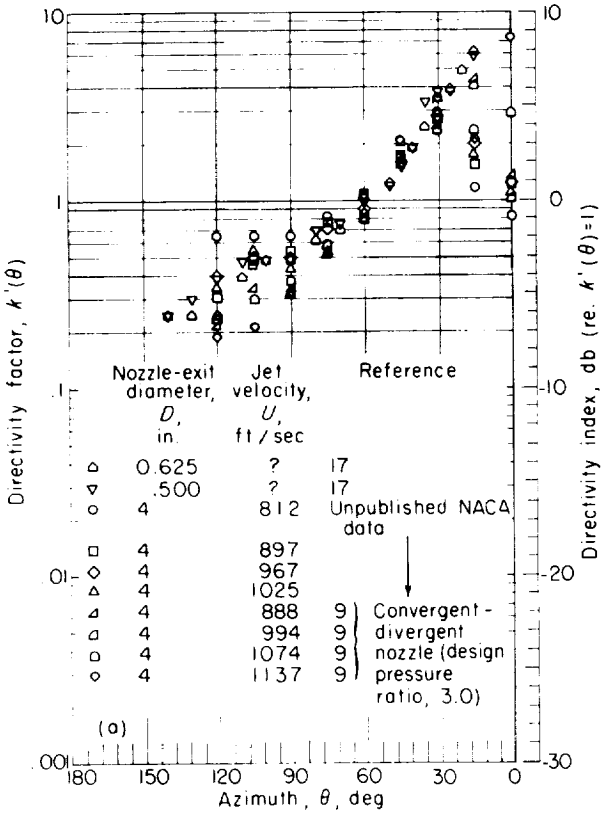

(a) Air jets.

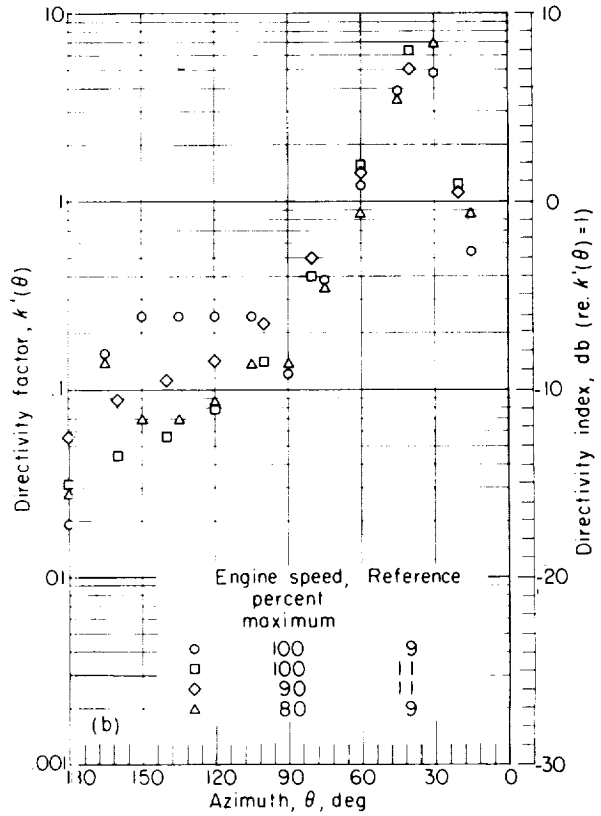

(b) Turbojet engines.

FIGURE 16.—Directivity functions for subsonic jets.

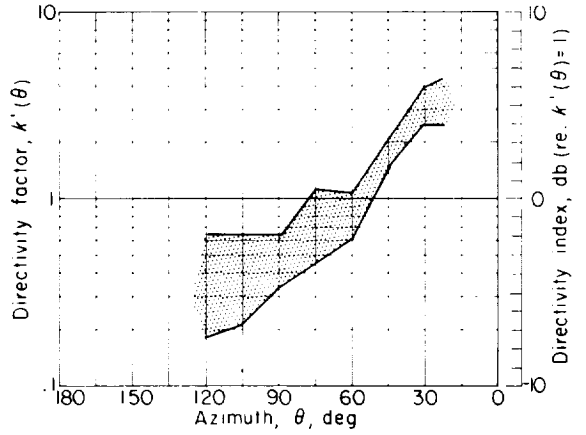

FIGURE 17.—Collective directivity pattern for subsonic air jets (refs. 9, 17, unpublished NACA data, and present tests).

SUMMARY OF RESULTS

From a correlation of new and previously published data on acoustic far fields of jets issuing from circular nozzles, the following results were obtained:

1. For subsonic jets the relation between acoustic power and the geometric and fluid properties is adequately represented in terms of the Lighthill parameter. For engineering purposes, the value of the acoustic-power coefficient may be taken as $\approx 3\times 10^{-5}$. The acoustic-power–fluid-property relation appeared unaffected by variations of jet temperature throughout the range 30° to 1300° F.

2. For supersonic jets, no adequate relation exists for predicting total acoustic power from the

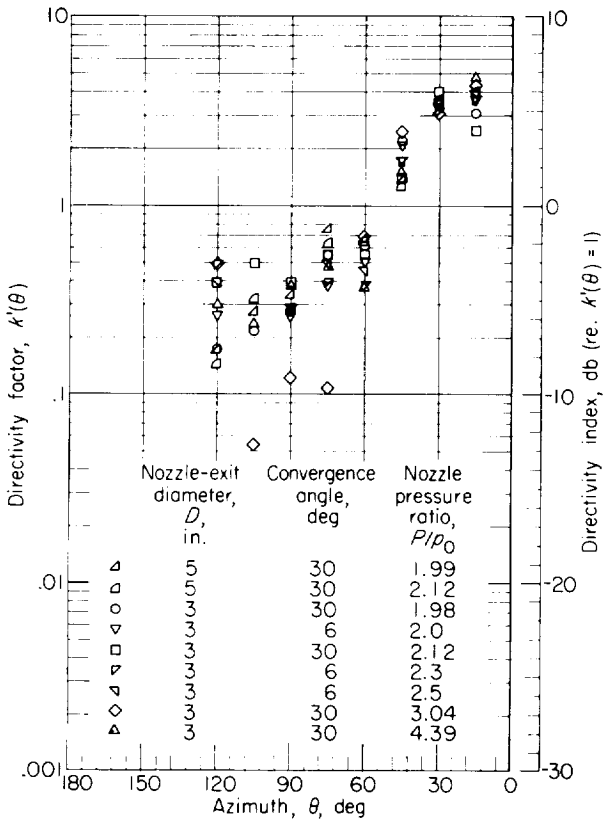

FIGURE 18.—Directivity functions for supersonic air jets. Present tests.

geometric and fluid properties over a wide range of flow conditions.

3. Dimensionless representations for the total-acoustic-power spectrum, directivity factor, and local mean-square-pressure spectrum derived herein were found to provide generally good correlation of noise data. In many instances, correlations for subsonic and supersonic jets were identical. Effects of nozzle size and similarity and of jet temperature on the correlations were noted in certain instances.

4. In the presence of discrete-frequency whistling, the previous correlations fail near the whistle frequency. Whistling appears to be a characteristic of small, cold, choked jets only.

5. The probability-density of acoustic pressure was found to be approximately normally distributed, even in the presence of discrete-frequency whistles.

6. In general, wind was the biggest obstacle in obtaining noise data suitable for studying similarity, particularly at the lower noise levels and acoustic frequencies. Microphone calibration differences and nozzle dissimilarity were suspected as the prominent sources of divergence of total-power determinations.

LEWIS RESEARCH CENTER
NATIONAL AERONAUTICS AND SPACE ADMINISTRATION
CLEVELAND, OHIO, *June 11, 1959*

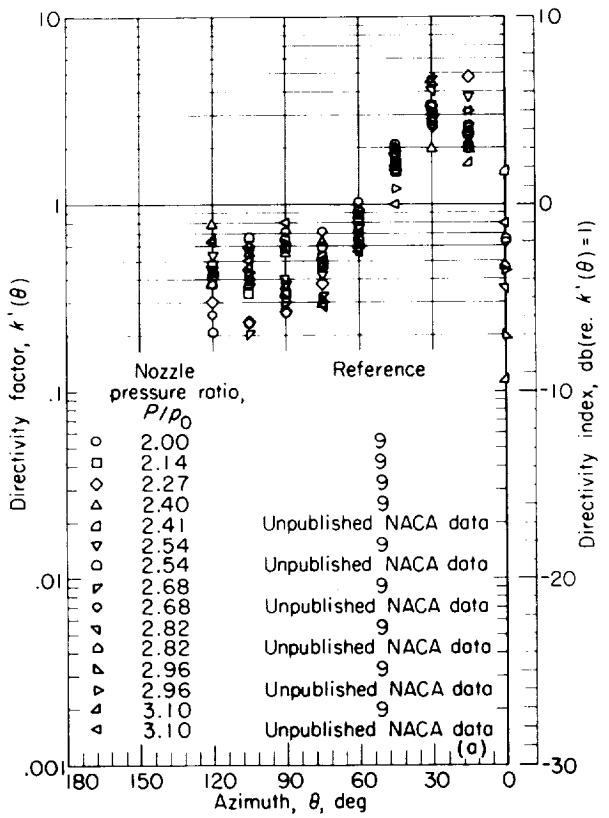

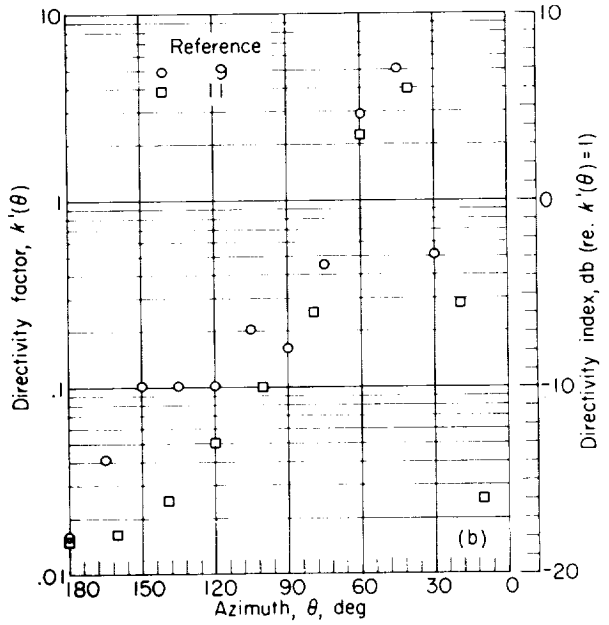

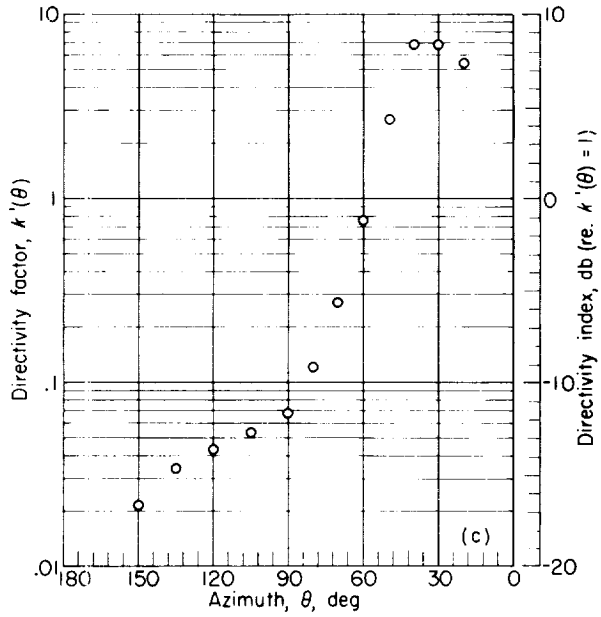

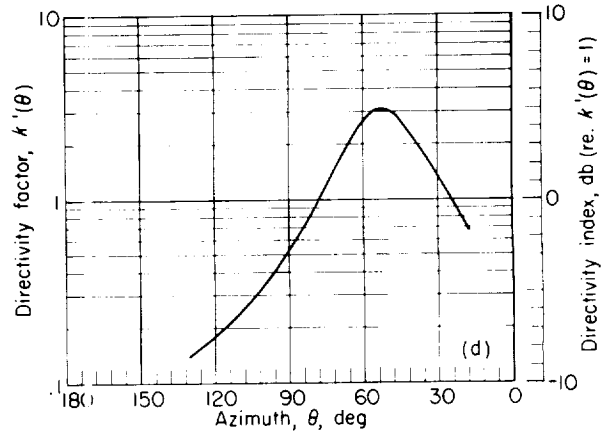

(a) Air jets. Nozzle-exit diameter, 4 inches. Data from reference 9 for convergent-divergent nozzle (design pressure ratio, 3.0); unpublished NACA data for convergent nozzle (convergence angle, 30°).

(b) Afterburning turbojet engines. For data from reference 9; nozzle-exit diameter, 2.33 feet; jet velocity, 2590 feet per second.

(c) Hot air jet (fig. 6 of ref. 20). Nozzle-exit diameter, 2.7 inches; nozzle pressure ratio P/p_0, 2.27; jet temperature 1437° R.

(d) Average for rockets with convergent-divergent nozzles (fig. 46 of ref. 2).

FIGURE 19.—Directivity functions for supersonic jets.

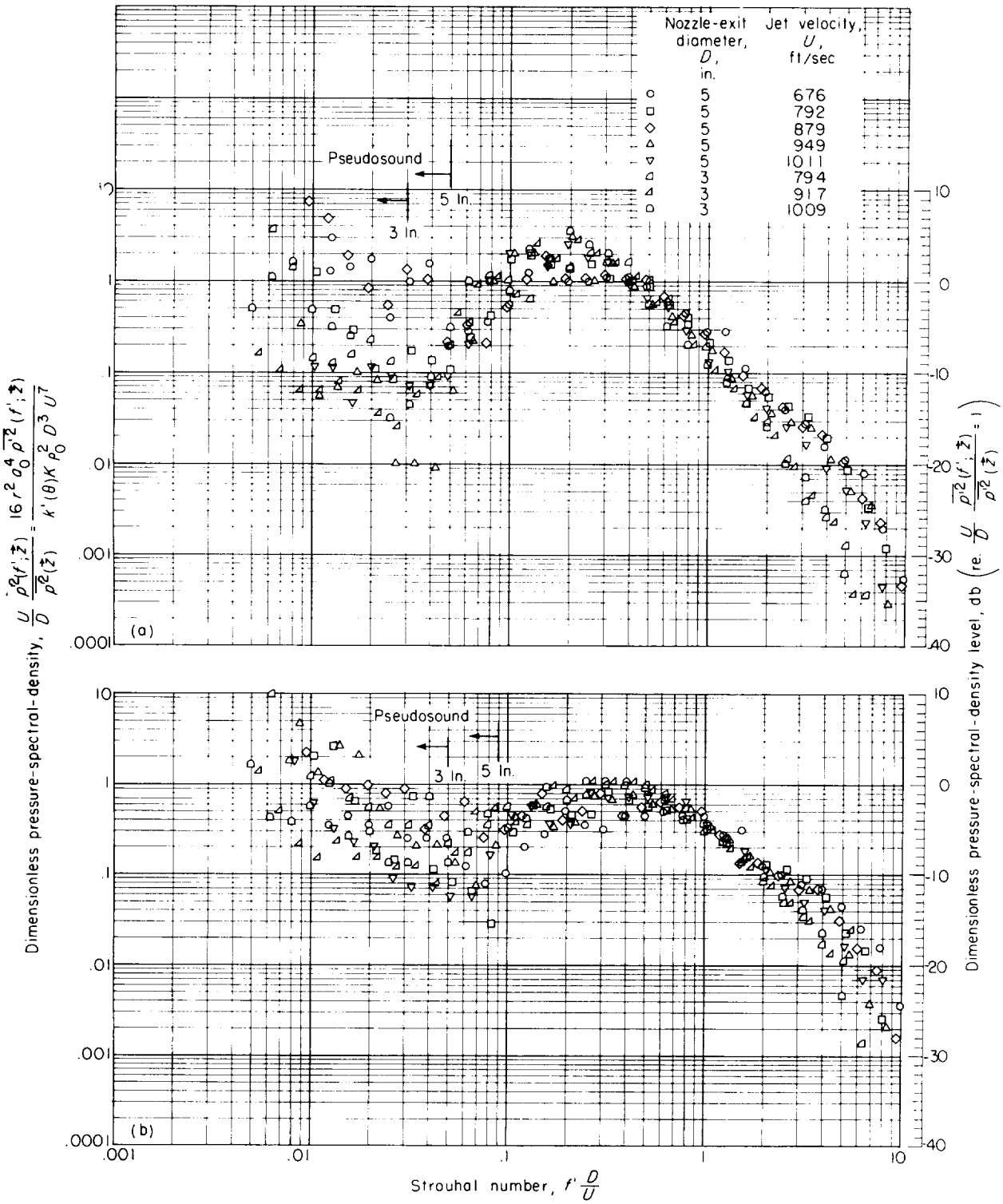

(a) Azimuth, 30°.
(b) Azimuth, 90°.

FIGURE 20.—Dimensionless pressure-spectral-density functions for subsonic air jets. Present tests. Radius r, 50 feet.

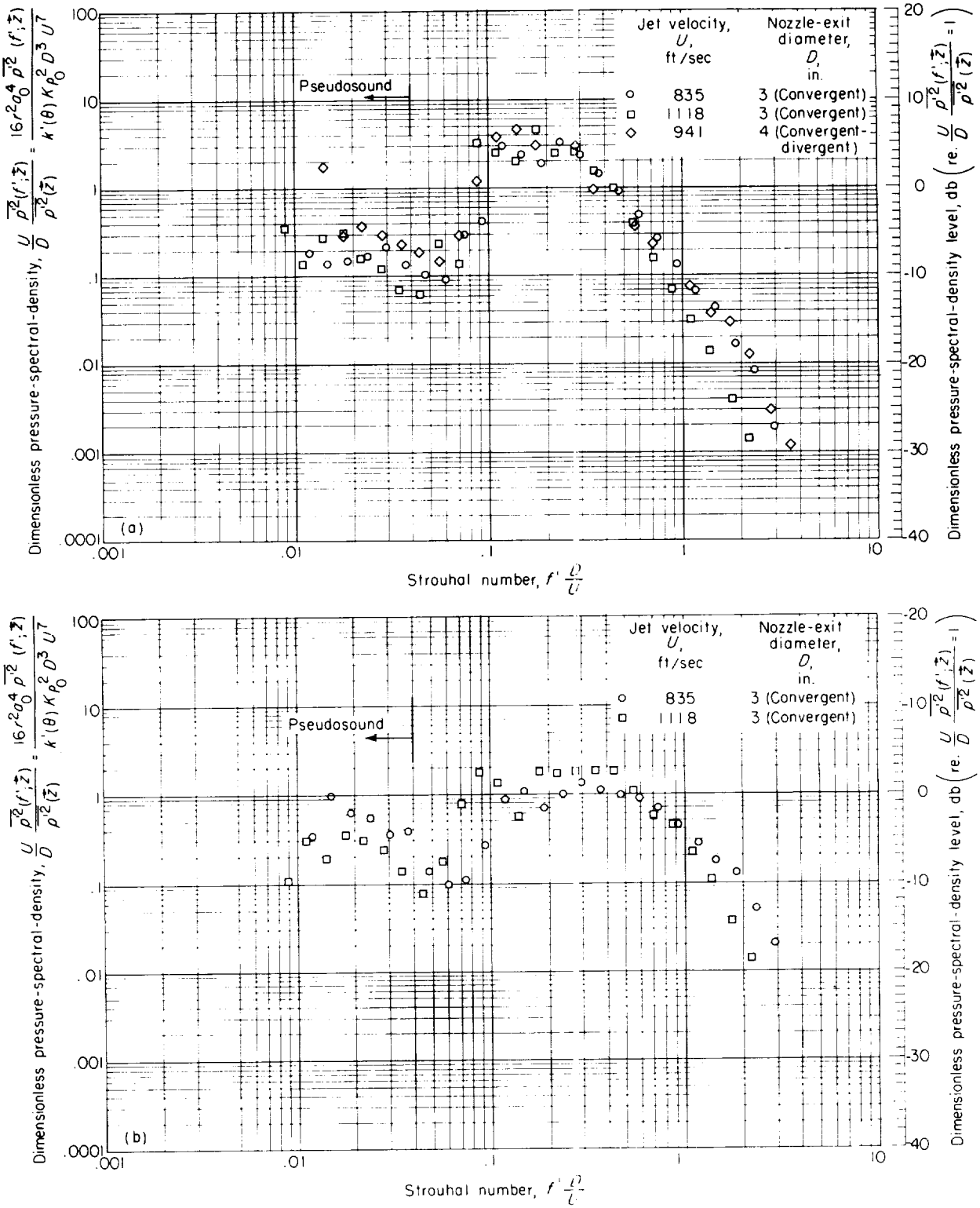

(a) Air jet. Azimuth, 30°; radius r, 50 feet. (b) Air jet. Azimuth, 90°; radius r, 50 feet.

FIGURE 21.—Dimensionless pressure-spectral-density functions for subsonic jets (ref. 9).

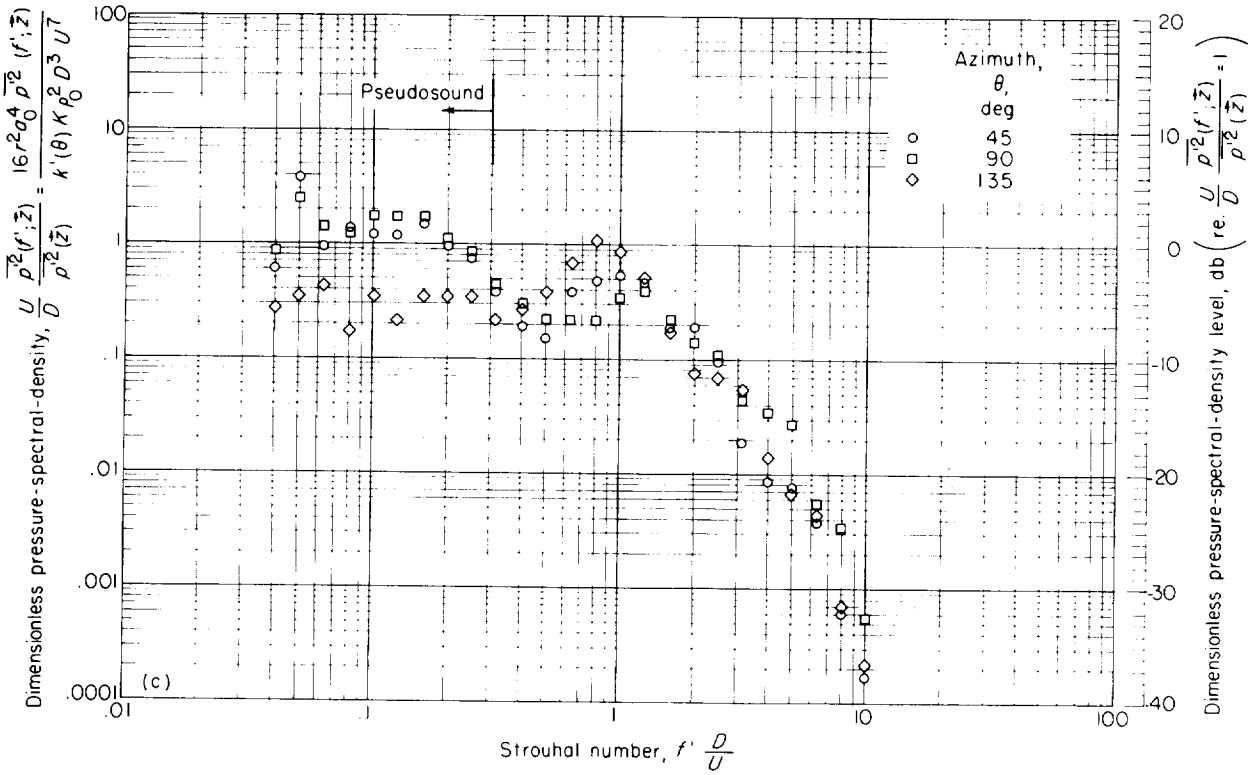

(c) Turbojet engine. Nozzle-exit diameter, 1.855 feet; jet velocity, 1850 feet per second; nozzle pressure ratio P/p_0, 2.2; radius r, 200 feet.

FIGURE 21.—Concluded. Dimensionless pressure-spectral-density functions for subsonic jets (ref. 9).

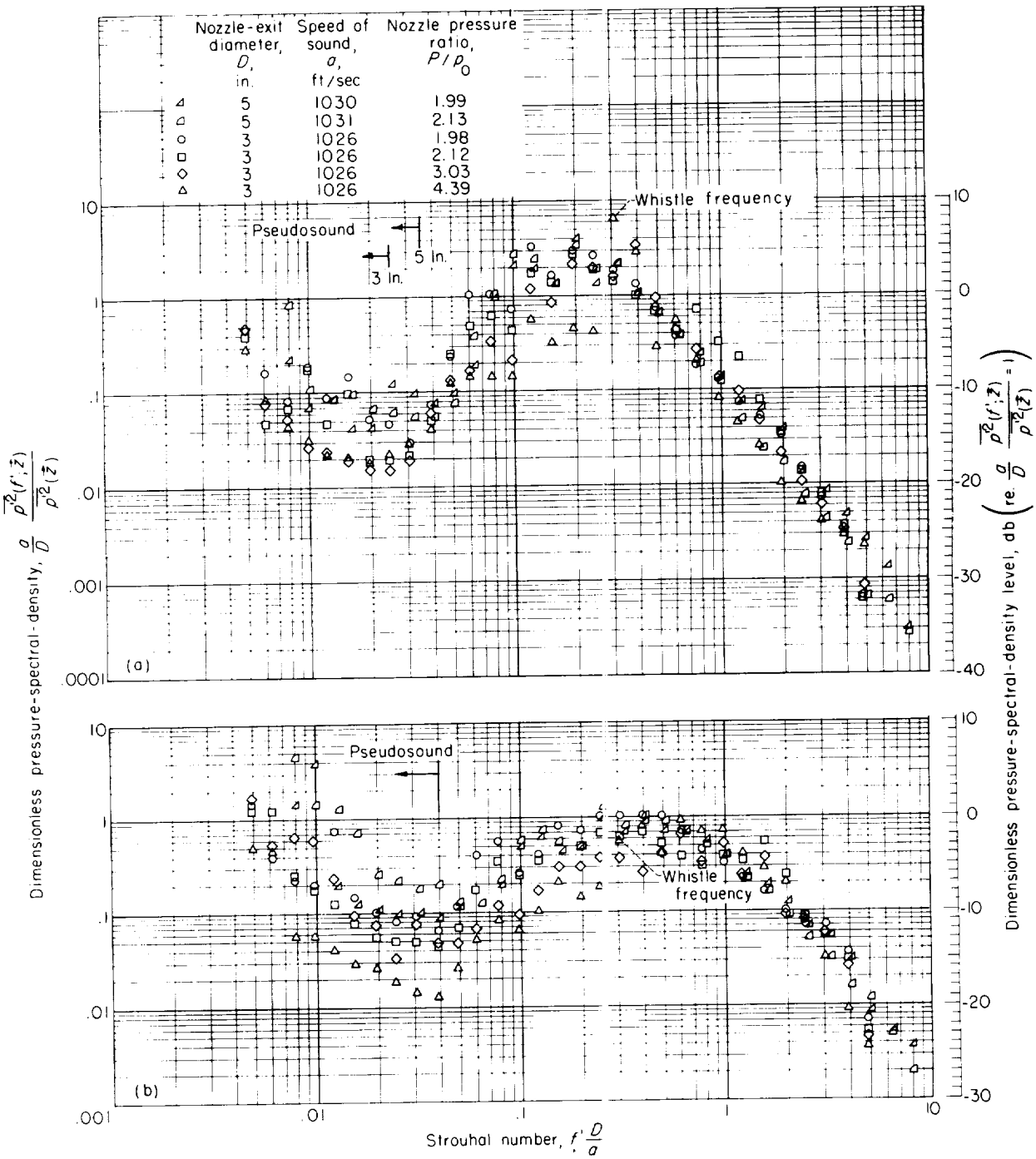

(a) Azimuth, 30°.
(b) Azimuth, 90°.

FIGURE 22.—Dimensionless pressure-spectral-density functions for supersonic air jets. Present tests. Radius r, 50 feet.

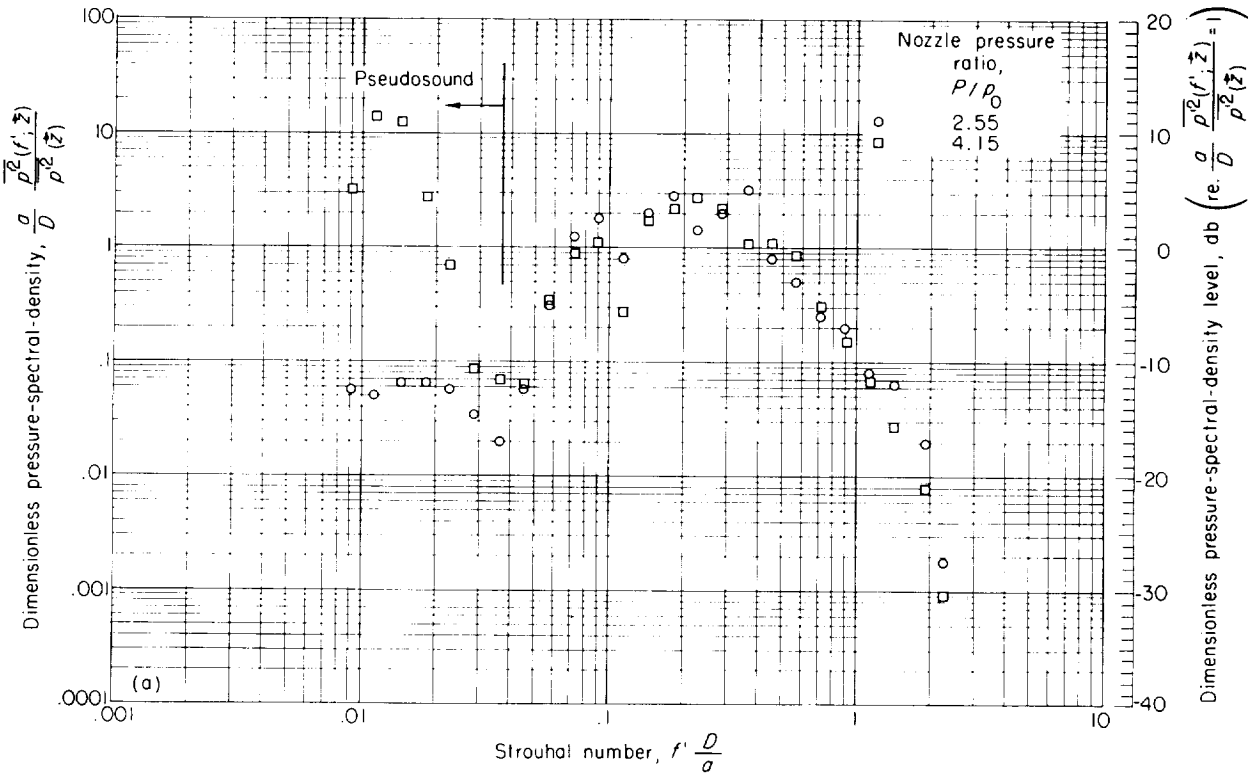

(a) Air jet (from fig. 11 of ref. 9). Azimuth, 30°; nozzle-exit diameter, 3 inches; radius r, 50 feet; speed of sound a, 1118 feet per second.

FIGURE 23. Dimensionless pressure-spectral-density functions for supersonic jets.

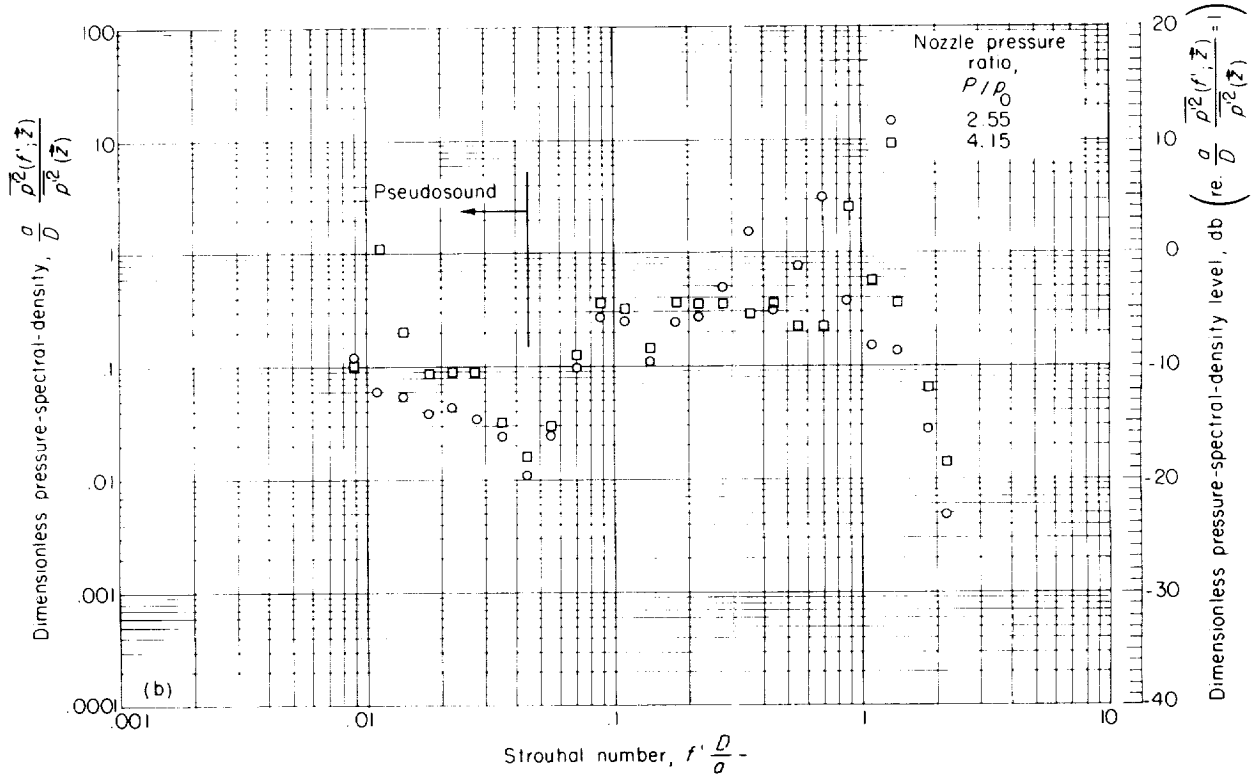

(b) Air jet (from fig. 11 of ref. 9). Azimuth, 90°; nozzle-exit diameter, 3 inches; radius r, 50 feet; speed of sound a 1118 feet per second.

FIGURE 23. Continued. Dimensionless pressure-spectral-density functions for supersonic jets.

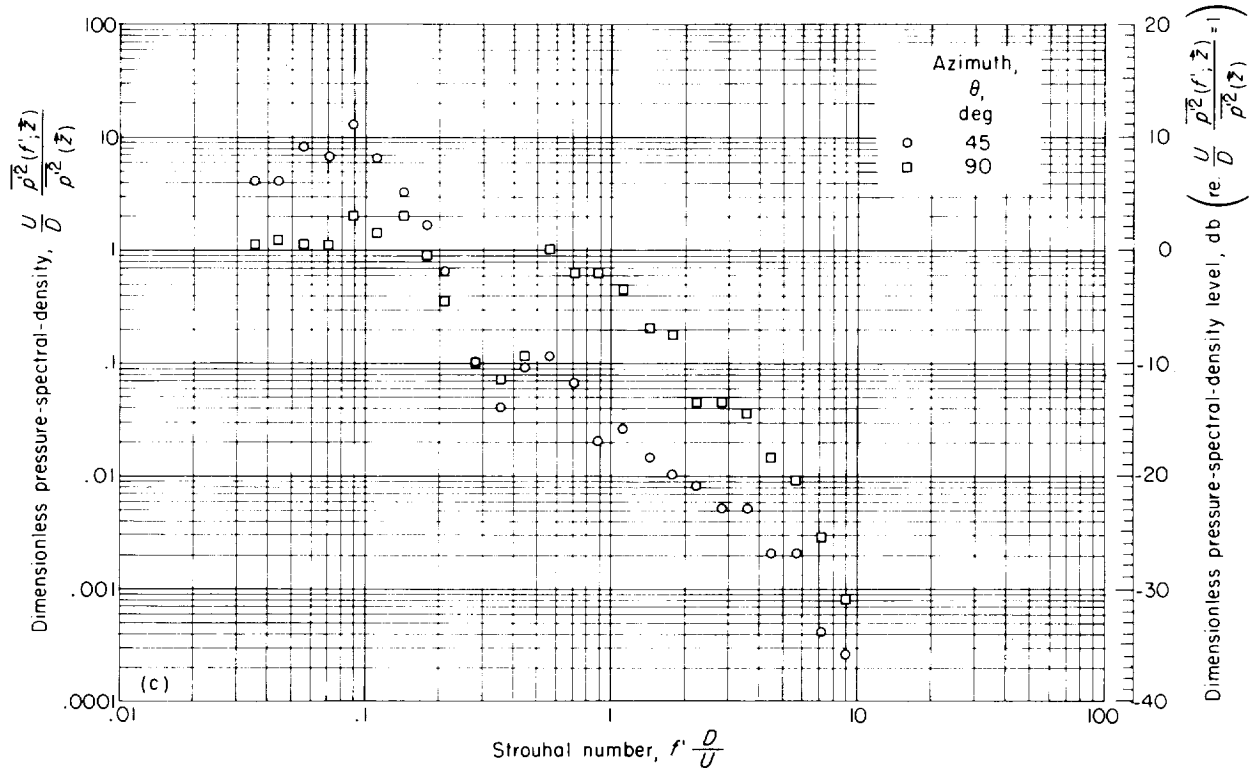

(c) Afterburning turbojet engine (ref. 9). Nozzle-exit diameter, 2.33 feet; jet velocity, 2590 feet per second; radius r, 400 feet.

FIGURE 23.—Concluded. Dimensionless pressure-spectral-density functions for supersonic jets.

532585 -60 — -5

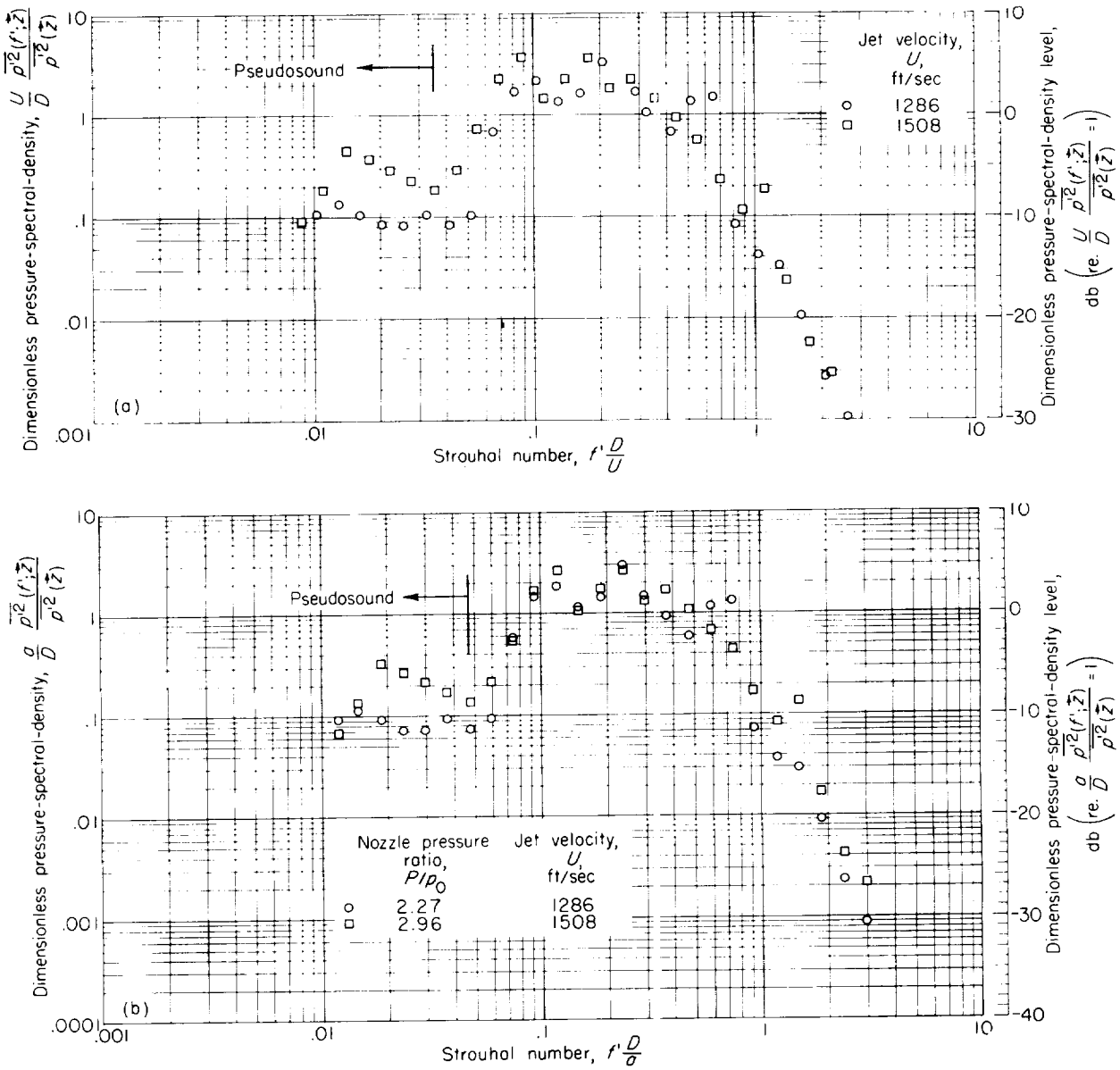

(a) Similarity based on jet velocity U.
(b) Similarity based on speed of sound a.

FIGURE 24. Dimensionless pressure-spectral-density functions for convergent-divergent nozzle (design pressure ratio, 3.0). Nozzle-exit diameter, 4 inches; radius r, 50 feet; azimuth, 30°.

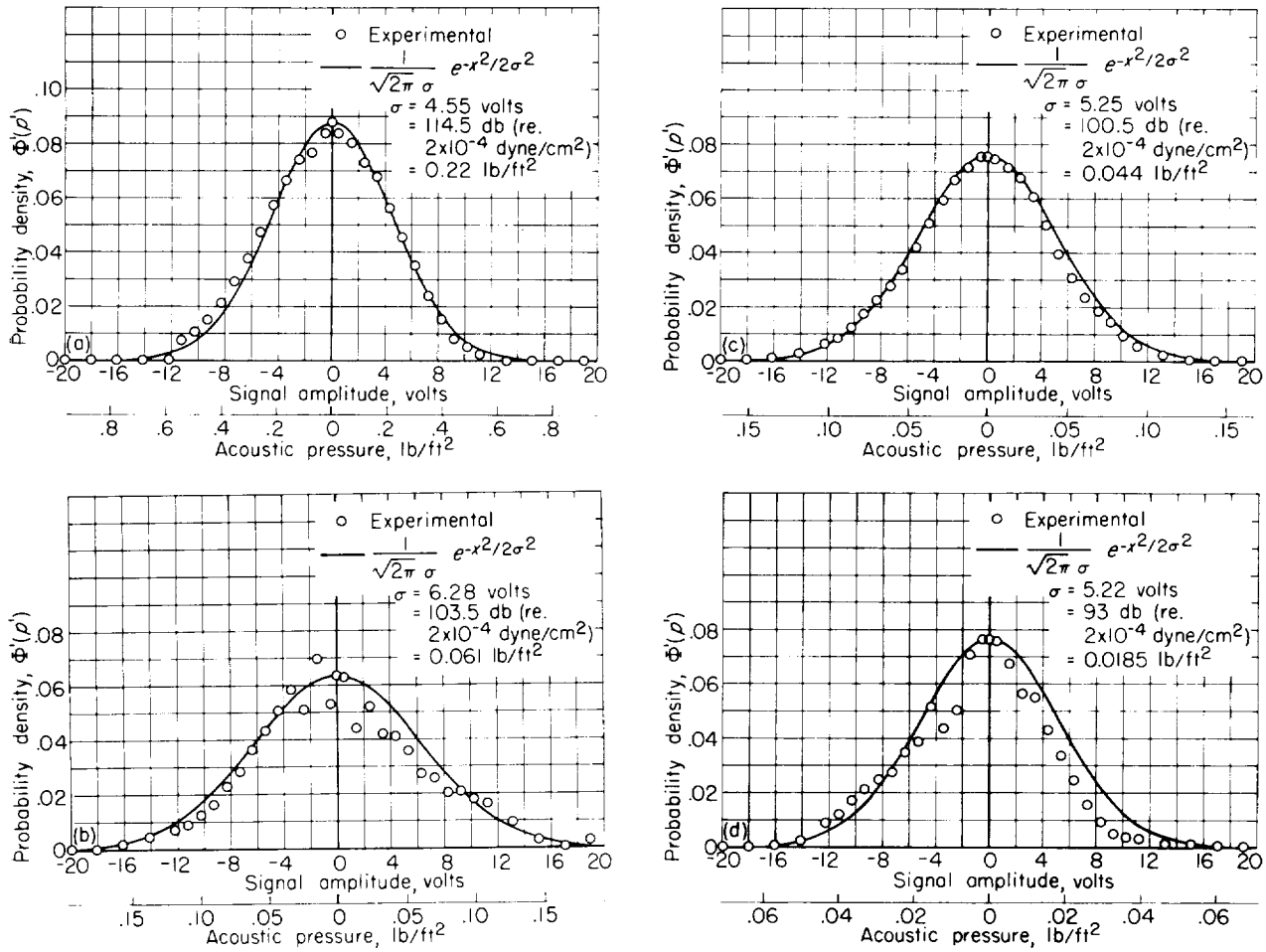

(a) Nozzle-exit diameter, 3 inches; azimuth, 30°; jet velocity, 917 feet per second.

(b) Nozzle-exit diameter, 3 inches; azimuth, 120°; jet velocity, 917 feet per second.

(c) Nozzle-exit diameter, 5 inches; azimuth, 30°; jet velocity, 879 feet per second.

(d) Nozzle-exit diameter, 5 inches; azimuth, 120°; jet velocity, 879 feet per second.

FIGURE 25.—Acoustic-pressure probability-density for subsonic air jets. Radius r, 50 feet.

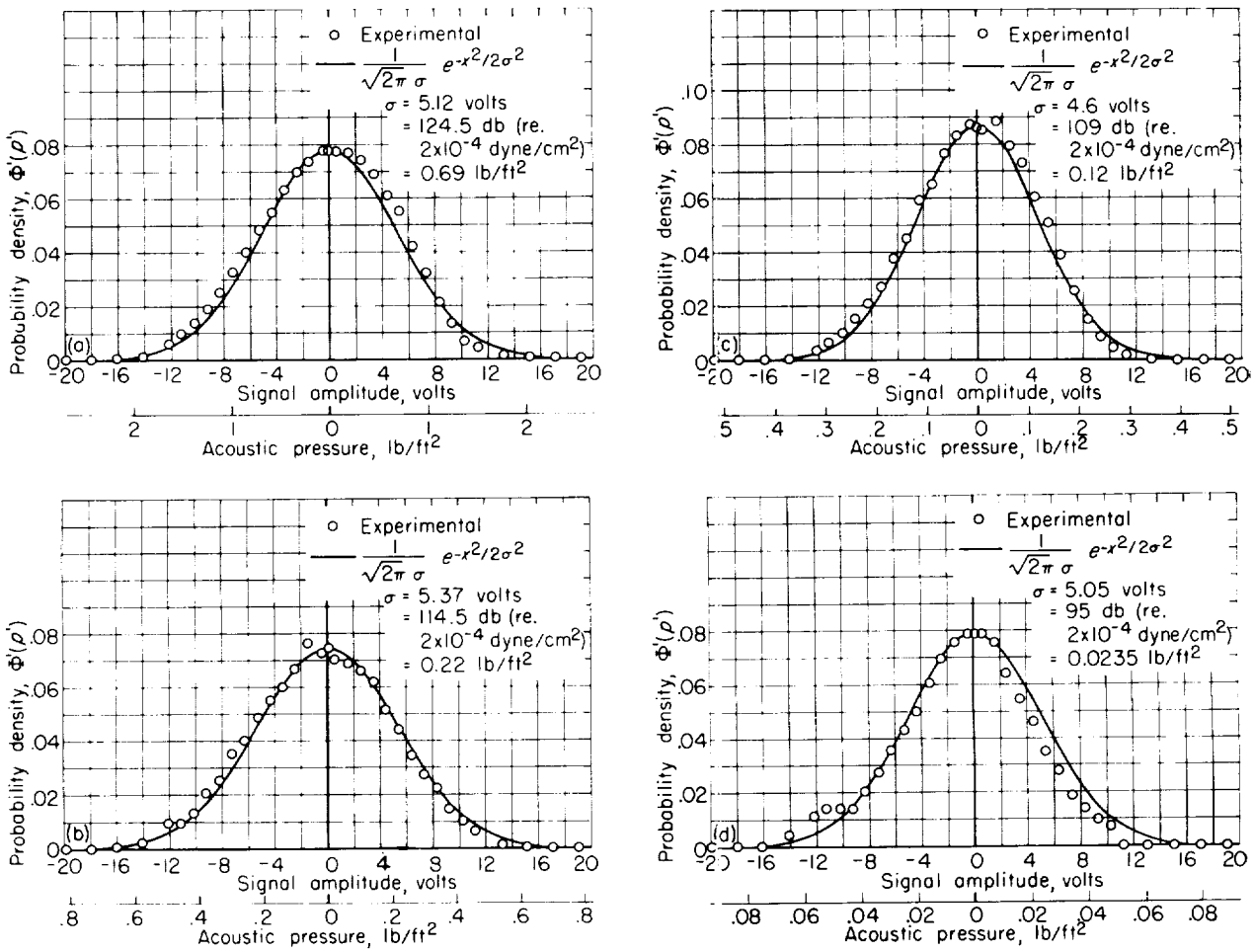

(a) Nozzle-exit diameter, 3 inches; azimuth, 30°; nozzle pressure ratio P/p_0, 2.12; speed of sound a, 1026 feet per second.

(b) Nozzle-exit diameter, 3 inches; azimuth, 120°; nozzle pressure ratio P/p_0, 2.12; speed of sound a, 1026 feet per second.

(c) Nozzle-exit diameter, 5 inches; azimuth, 30°; nozzle pressure ratio P/p_0, 2.13; speed of sound a, 1030 feet per second.

(d) Nozzle-exit diameter, 5 inches; azimuth, 120°; nozzle pressure ratio P/p_0, 2.13; speed of sound a, 1030 feet per second.

FIGURE 26.—Acoustic-pressure probability-density for supersonic air jets. Radius r, 50 feet.

APPENDIX A

SYMBOLS

A	nozzle-exit area
A^*	cross-sectional area of supersonic jet at effective sonic plane downstream of exit
a	speed of sound
a^*	critical speed of sound, critical speed of sound in supersonic jet at effective sonic plane downstream of exit
C_d	nozzle discharge coefficient
C_V	nozzle velocity coefficient
D	nozzle-exit diameter
D^*	diameter of supersonic jet at effective sonic plane downstream of exit
F	thrust
f	frequency, cps
f'	geometric-mean frequency of filter, cps
f^*	characteristic frequency, cps
$g(P/p_0)$	acoustic power function for supersonic-flow region upstream
I	acoustic intensity
K	acoustic-power coefficient
k	acoustic-pressure coefficient
k'	acoustic-directivity factor
k'_c	acoustic-directivity factor for supersonic-flow region
L	Lighthill parameter, $\rho_0 A U^8/a_0^5$
L^*	modified Lighthill parameter, $\rho_0 A^* a^{*8}/a_0^5$
L_i	modified Lighthill parameter, $\rho_0 A U_i^8/a_0^5$
l	characteristic length
$\dot{m}$	mass-flow rate
P	plenum total pressure
PWL	acoustic-power level$=10 \log (W/w_0)$, db (w_0=re. acoustic power$=10^{-13}$ watt)
p	mean static pressure
p'	acoustic pressure
p'	acoustic pressure resulting from supersonic jet
$p'(f;\vec{z})$	local acoustic pressure-per-cycle-per-second
$p'(\vec{z})$	local over-all acoustic pressure
r	radius of control sphere centered at nozzle exit, $r \gg \lambda$
S	area of control sphere
T_{ij}	equivalent stress tensor
t	time
U	characteristic velocity
U_e	effective nozzle-exit velocity
U_i	ideal nozzle-exit velocity
U_m	mean nozzle-exit velocity
u_ξ	local nozzle-exit velocity
u'	turbulent velocity
W	total acoustic power
W_c	total-acoustic-power contribution from supersonic-flow region
W_t	total acoustic power resulting from supersonic jet
$w(f)$	acoustic power-per-cycle-per-second (acoustic power-spectral-density)
$w_c(f)$	acoustic power-per-cycle-per-second generated by supersonic-flow region
$w_t(f)$	acoustic power-per-cycle-per-second generated by supersonic jet
x_i	coordinates of acoustic far-field points
y_i	coordinates of points within turbulence region
$\vec{z}$	$\vec{x}-\vec{y}$
α	directivity correction coefficient for supersonic-flow region upstream
θ	azimuth with respect to direction of jet flow, deg
λ	acoustic wavelength
μ_n	n^{th} central moment about p_0, $\int_{-\infty}^{\infty} p'^n \Phi'(p')\,dp'$
ξ,η,ζ	coordinates (see fig. 1)
ρ	mean density
ρ'	density fluctuation
σ	standard deviation, $\sqrt{\overline{p'^2}}$
Φ'	probability-density function
φ	normal-probability-density function, $\varphi(p')=\frac{1}{\sqrt{2\pi}\,\sigma} e^{-\frac{1}{2}\left(\frac{p'}{\sigma}\right)^2}$
$\langle\ \rangle$	space average

Subscripts:

i, j	integers; $i, j=1, 2, 3$
max	maximum
0	ambient value

Superscripts:

—	time average
→	vector

APPENDIX B

SIMILARITY RELATIONS

TOTAL ACOUSTIC POWER

The density fluctuations in the acoustic far field, given by

$$\rho'(\vec{x}) \approx \frac{1}{4\pi a_0^2} \frac{x_i x_j}{x^3} \int \frac{1}{a_0^2} \frac{\partial^2}{\partial t^2} T_{ij}\left(\vec{y}, t - \frac{|\vec{x}-\vec{y}|}{a_0}\right) d\vec{y} \tag{4}$$

are expressed in dimensional representation by

$$\rho' \propto \frac{f^{*2}\rho_0 u'^2 l^3}{a_0^4 r} \tag{B1}$$

where f^* is a characteristic frequency, r is a nominal distance separating the turbulent region and acoustic-field point, l is a characteristic dimension of the turbulent region, and

$$\text{Dimension } \frac{\partial^2}{\partial t^2} = \text{Dimension } f^{*2}$$

$$T_{ij} \approx \rho_0 u_i' u_j' \text{ (ref. 4)}$$

$$\text{Dimension } \rho_0 u_i' u_j' = \text{Dimension } \rho_0 u'^2$$

For acoustic disturbances,

$$p' \approx a_0^2 \rho'$$

so that the instantaneous acoustic pressure is represented by

$$p' \propto \frac{f^{*2}\rho_0 u'^2 l^3}{a_0^2 r} \tag{B2}$$

Substituting this result in equation (3) yields

$$I \propto \frac{f^{*4}\rho_0 (\overline{u'^2})^2 l^6}{a_0^5 r^2} \tag{B3}$$

which, when substituted in equation (2), finally yields

$$W \propto f^{*4}\rho_0 (\overline{u'^2})^2 l^6 a_0^{-5} \tag{B4}$$

for the total acoustic power.

By assuming, in general,

$$f^* \frac{l}{U} \approx \text{const.} \tag{B5}$$

$$\overline{u'^2} \propto U^2 \tag{B6}$$

and

$$l^2 \propto A \tag{B7}$$

equation (B4) becomes

$$W \propto \rho_0 A U^8 a_0^{-5} \tag{B8}$$

This may be written as an equality (eq. (5)) by inserting a proportionality constant K, the acoustic-power coefficient.

(The form of eq. (5) might also have been deduced from physical reasoning and dimensional analysis without resorting to the use of eq. (4). In this case, the result is

$$W \propto \rho_0 A U^\beta a^{3-\beta}$$

where β is a constant to be determined by experiment.)

Consider, now, the acoustic power radiated by a flow region containing shock waves. If it is assumed that the noise production of supersonic jets is strongly influenced by the presence of shock waves, Ribner's theory of shock-turbulence interaction may be applicable. The theory, however, relates to near-field, rather than far-field acoustic pressures. Thus, reconsider the relation for acoustic power radiated by a region of flow. In the far field, at a sphere surrounding the flow,

$$W_c = \int_S \frac{\langle \overline{p'^2}(r) \rangle}{\rho_0 a_0} ds \propto \frac{\langle \overline{p'^2}(r) \rangle r^2}{\rho_0 a_0}$$

by virtue of equations (2) and (3) and dimensional considerations. Because W_c must be independent of r, consider

$$\langle \overline{p'^2}(r) \rangle \propto \langle \overline{p'^2}(l) \rangle \frac{l^2}{r^2}$$

where $\langle\overline{p'^2}(l)\rangle$ represents a characteristic mean-square pressure in the near field and is associated with the characteristic dimension l. Then,

$$W_c \propto \frac{\langle\overline{p'^2}(l)\rangle l^2}{\rho_0 a_0} \tag{B9}$$

From the data of reference 9, the term in l^2 obviously corresponds to A. There is some question as to the relation between $\langle\overline{p'^2}(l)\rangle$ and the fluid variables. This pressure fluctuation may be related to a characteristic velocity, as in Lighthill's theory of aerodynamic noise. However, for the present, assume Ribner's theory is applicable. Consider proportionality (6). For near-field-pressure fluctuations behind a shock wave, assume $\langle\overline{p'^2}(l)\rangle \propto \overline{p'^2}(\xi-\xi_0 \leqq \lambda)$. In equation (6), $\overline{u'^2}/a^{*2}$ may be regarded as an unknown, probably nonlinear, function of the isentropic stream Mach number associated with the nozzle pressure ratio P/p_0. Also, as a first guess, the mean static pressure p downstream of the shock will be set equal to the ambient pressure p_0. Thus, proportionality (B9) becomes

$$W_c = \frac{p_0^2 A}{\rho_0 a_0} g(P/p_0) \tag{B10}$$

where $g(P/p_0)$ is a function of P/p_0 to be determined by experiment. Because $W_c=0$ for $P/p_0 \leqq 1.89$, it follows necessarily that $g=0$ for this condition.

(By using the same variables and, as before, making the assumption that $\overline{u'^2}/a^{*2}$ is a nonlinear function of P/p_0, the equation for W_c obtained by dimensional analysis is

$$W_c = \left(\frac{p}{\rho a^2}\right)^{\delta} \rho a^3 A g'(P/p_0)$$

where g' is an unknown function of P/p_0, and, δ is a constant to be determined experimentally. This result is identical to eq. (B10) if $\delta=2$.)

POWER SPECTRUM

For supercritical pressure ratios the total-power spectrum can be synthesized from the power spectrum components radiated by the subsonic- and supersonic-flow regions. Thus,

$$\frac{1}{W_t}\int_0^\infty w_t(f)\mathrm{d}f = \frac{1}{W_t}\left(\int_0^\infty w(f)\mathrm{d}f + \int_0^\infty w_c(f)\mathrm{d}f\right) = 1$$

or

$$\frac{1}{W_t}\left\{\int_0^\infty \left[\frac{a^* w(f)}{D^*}\right]\frac{D^*}{a^*}\mathrm{d}f + \int_0^\infty \left[\frac{a w_c(f)}{D}\right]\frac{D}{a}\mathrm{d}f\right\} = 1 \tag{12}$$

DIRECTIVITY

By making the same assumptions regarding the turbulence, namely assumptions (B5) to (B7), as were made in deriving equation (5) for the total power W, an expression results for the average value of the mean-square acoustic pressure on a sphere of nominal radius r surrounding the turbulent region:

$$\langle\overline{p'^2}(r)\rangle = k\frac{\rho_0^2 A U^8}{a_0^4 r^2} \tag{B11}$$

where k is an average acoustic-pressure coefficient analogous to K. Let $k'(\theta)$ represent a directivity factor, a function of θ only, for jets having circular cross sections. Then, at any field point on the spherical surface, the local mean-square acoustic pressure is given by

$$\overrightarrow{\overline{p'^2}}(z) = k'(\theta) k \frac{\rho_0^2 A U^8}{a_0^4 r^2} \tag{B12}$$

Taking the ratio of equation (B12) to (B11) yields

$$k'(\theta) = \overrightarrow{\overline{p'^2}}(z)/\langle\overline{p'^2}(r)\rangle \tag{B13a}$$

$$= \overrightarrow{I}(z)/\langle I(r)\rangle \tag{B13b}$$

where the latter relation results by virtue of equation (3). Alternatively, by definition,

$$\langle\overline{p'^2}(r)\rangle = \frac{1}{S}\int_S \overrightarrow{\overline{p'^2}}(z)\mathrm{d}s \tag{B14}$$

or, by considering equations (2) and (3),

$$\langle\overline{p'^2}(r)\rangle = \frac{\rho_0 a_0 W}{4\pi r^2} \tag{B15a}$$

$$= K\frac{\rho_0^2 A U^8}{4\pi r^2 a_0^4} \tag{B15b}$$

Taking the ratio of equation (B11) to (B15b),

$$k = K/(4\pi)$$

Substituting expression (B13a) for $\langle\overline{p'^2}(r)\rangle$ in equations (B15a) and (B15b) yields equations (13) and (14), respectively.

By replacing W in equation (13) by the expression for W_t in equation (8a), and $k'(\theta)$ by a new factor $k'_t(\theta)$, an equation for $\overline{p'^2}(\vec{z})$ associated with supersonic jets is obtained:

$$\overline{p'^2_t}(\vec{z})=k'_t(\theta)\,\frac{\rho_0 a_0}{4\pi r^2}\left[KL^*+\frac{p_{0^*}^2-1}{\rho_0 a_0}\,g(P/p_0)\right] \quad \text{(B16)}$$

Because $k'_t(\theta)=k'(\theta)$ for the subsonic contribution, equation (B16) can be rewritten in the form

$$\overline{p'^2}(\vec{z})=k'(\theta)\,\frac{\rho_0 a_0}{4\pi r^2}\,KL^*+k'_c(\theta)\,\frac{p_{0^*}^2-1}{4\pi r^2}\,g(P/p_0) \quad \text{(B17a)}$$

or

$$\overline{p'^2}(\vec{z})=k'(\theta)\left[\frac{\rho_0 a_0}{4\pi r^2}\,KL^*+\alpha\,\frac{p_{0^*}^2-1}{4\pi r^2}\,g(P/p_0)\right] \quad \text{(B17b)}$$

Equations (15a) and (15b) immediately follow from equations (B17a) and (B17b), respectively, by rewriting L^* in terms of the flow and geometric variables.

APPENDIX C

EXPERIMENTAL DIFFERENCES AND ERRORS

Characteristic differences between the different experiments include

(1) the jet
  (a) dynamical similarity
  (b) definition of jet velocity
(2) experimental conditions
  (a) radius of measurement compared to distance to acoustic far field (free-field tests)
  (b) totality of measurement directions (free-field tests)
  (c) angular separation of measurement directions (free-field tests)
  (d) surface reflections (quasi-free-field tests)
  (e) reverberant chamber characteristics (reverberation tests)
  (f) wind (outdoor tests)
  (g) secondary-noise sources (engine tests)
(3) instrumentation
  (a) frequency pass-band compared to acoustic-spectrum bandwidth
  (b) signal averaging characteristic
  (c) calibration error

Test conditions relating to these factors are outlined in table II. Estimates of the induced errors are listed in table III. The methods by which the errors were estimated are discussed below. The numbers and letters refer to the preceding listing.

(1) Because $W \propto U^8$, the definition of jet velocity that is selected for correlation purposes is important. In the tests reported, jet velocity was determined by at least three basically different methods (table I). Nozzle-pressure-ratio measurements lead to the "ideal" velocity U_i. Determining the ratio of jet thrust to jet-exhaust mass-flow rate yields the "effective" velocity,

$$U_e=\frac{F}{\dot{m}}=\frac{F}{\rho A C_d C_U U_i}$$

where

$$U_e=C_U U_i$$

(Pressure forces are assumed to be negligible.) Finally, measuring the total-pressure profile at the nozzle exit permits the determination of "local" velocity $u_\xi(\eta,\zeta)$, hence the "mean" velocity

$$U_m=\frac{1}{A}\int_A u_\xi \, d\eta \, d\zeta$$

where

$$U_m=U_e$$

Since equation (4) is assumed to be valid for each point throughout the flow $\frac{1}{A}\int_A u_\xi^8 \, d\eta \, d\zeta$ might provide the best correlation (ref. 23). The more readily determined alternative is U_m, or U_e. If correlations are assumed to be based on U_e, then those correlations originally based on U_i must be adjusted according to the relation

$$L=C_U^8 L_i$$

where L is Lighthill's parameter based on U_e, and L_i is the same parameter based on U_i.

Except for the 3-inch-diameter nozzle used in the present tests, data on C_U were not available for the other nozzles. Estimates for the other nozzles were based on knowledge of the nozzle configurations and the fact that, for a nozzle with good thrust characteristics, $C_U \approx 0.98$ in the high subsonic-velocity range.

The previous consideration of velocity distribution should effectively account for similarity effects also.

(2) Effects (a) and (b) were computed and found to be negligible.

(c) This effect might introduce an error as large as 1 or 2 decibels in comparing the total power from experiments for which the measurement angles were different. The effect is, of course, most significant near the angle for which the acoustic intensity is maximum. No attempt was made to evaluate this error.

(d) Surface reflection corrections were based on theoretical computations according to reference 21.

(e) Room reverberation characteristics were reported in reference 18, but not in reference 10. As a result, the systematic error of total-power measurements reported in reference 10 may have been of the order of 1 decibel (personal communication from Mr. George B. Towle of United Aircraft Corp.).

(f) The effect of wind and atmospheric turbulence on measured acoustic pressures tends to be random unless the wind impinges on the microphone. Then, an additional fluctuating pressure is added to the acoustic pressure. The additional pressure is independent of jet velocity and, hence, would tend to reduce the slope of curves of W as a function of L. The magnitude of the wind effect was evaluated from its effect on power spectra. The added pressure is predominant at low acoustic frequencies. In the tests described in reference 19, the low-frequency end of the spectrum ($<$225 cps) was disregarded. In the tests reported in reference 11 a microphone windscreen was used, whereas in the present tests over-all sound pressures were measured during minimum wind conditions.

(3) (a) The frequency-pass-band correction was based on knowledge of the power spectrum. By determining on the basis of many measured spectra the shape of the dimensionless spectrum, the neglected power associated with any particular spectrum resulting from a deficiency in the total accepted pass-band could be estimated.

(b) In all tests, except those reported in references 2 and 19, the meter-averaging characteristic for over-all measurements was mean-square or full-wave rectified. Theoretically, for a random noise input, the mean-square characteristic should yield a reading 1 decibel higher than that for full-wave rectification if both characteristics are assumed to yield the same reading for a sine-wave input (ref. 24, p. 453). This difference was verified for jet noise by comparing the readings of two meters having these characteristics. In addition, for a quasi-peak characteristic the level indication has been found to be 2 to 5 decibels higher than that for a rectifying characteristic in the case of jet noise (refs. 25, 26, and unpublished NACA tests). The divergent effect of the different characteristics is to cause differences of measured total power and distortions of spectra (ref. 25). For consistency with other tests, the correction applied in the published results in reference 19 was disregarded in this report. Thus, all results shown are uncorrected for meter characteristic.

(c) Calibration errors are indeterminate. It was concluded by applying all the preceding error corrections that this error could easily mask any additional systematic differences between different test results. In fact, calibration errors and wind effects were regarded as having the largest deleterious effect in correlating data.

In table III the reflection, wind, instrument frequency-pass-band, and meter-averaging corrections are with respect to W, whereas the velocity correction is with respect to L. Thus, an over-all correction is not obtained by simply adding all the individual contributions.

REFERENCES

1. Franken, Peter A.: Review of Information on Jet Noise. Noise Control, vol. 4, no. 3, May 1958, pp. 8–16.
2. Cole, J. N., et al.: Noise Radiation from Fourteen Types of Rockets in the 1,000 to 130,000 Pounds Thrust Range. TR 57-354, Aero. Medical Lab., WADC, Dec. 1957.
3. Chobotov, V., and Powell, A.: On the Prediction of Acoustic Environments from Rockets. GM-TR-90, Guided Missile Res. Div., The Ramo-Wooldridge Corp., Los Angeles (Calif.), June 3, 1957.
4. Lighthill, M. J.: On Sound Generated Aerodynamically. I General Theory. Proc. Roy. Soc. (London), ser. A, vol. 211, no. 1107, Mar. 20, 1952, pp. 564–587.
5. Lighthill, M. J.: On Sound Generated Aerodynamically. II Turbulence as a Source of Sound. Proc. Roy. Soc. (London) ser. A, vol. 222, no. 1148, Feb. 23, 1954, pp. 1–32.
6. Anderson, Arthur R., and Johns, Frank R.: Characteristics of Free Supersonic Jets Exhausting into Quiescent Air. Jet Prop., vol. 25, no. 1, Jan. 1955, pp. 13–15, 25.
7. Mull, Harold R., and Erickson, John C., Jr.: Survey of the Acoustic Near Field of Three Nozzles at a Pressure Ratio of 30. NACA TN 3978, 1957.
8. Rilner, H. S.: Shock-Turbulence-Interaction and the Generation of Noise. NACA Rep. 1233, 1955. (Supersedes NACA TN 3255.)
9. Callaghan, Edmund E., and Coles, Willard D.: Far Noise Field of Air Jets and Jet Engines. NACA Rep. 1329, 1957. (Supersedes NACA TN's 3590 and 3591.)
10. Tyler, John M., and Perry, Edward C.: Jet Noise. Preprint No. 287, SAE, 1954.
11. Clark, W. E., et al.: Noise Produced by Aircraft During Ground Run-Up Operations. TR 56-60, WADC, June 1957.
12. Bennett, W. R.: Methods of Solving Noise Problems. In Noise-Physical Sources and Methods of Solving Problems. Monograph 2624, Bell Telephone Sys-

tem, 1956. (See also Proc. IRE, vol. 44, no. 5, May 1956, pp. 609–638.)
13. Cramer, Harald: Mathematical Methods of Statistics. Princeton Univ. Press, 1946, pp. 221–224.
14. Carlson, Edward R., et al.: Special Electronic Equipment for the Analysis of Statistical Data. Proc. IRE, vol. 47, no. 5, pt. 1, May 1959, pp. 956–962.
15. Bolt, R. H., Lukasik, S. J., Nolle, A. W., and Frost, A. D., eds.: Handbook of Acoustic Noise Control. Vol. I. Physical Acoustics. TR 52–204, Aero. Medical Lab., WADC, Dec. 1952. (Contract AF 33(038)–20572.)
16. Fitzpatrick, H. M., and Lee, Robert: Measurements of Noise Radiated by Subsonic Air Jets. Rep. 835, The David W. Taylor Model Basin, Nov. 1952.
17. Lee, Robert: Free Field Measurements of Sound Radiated by Subsonic Air Jets. Rep. 868, The David W. Taylor Model Basin, Dec. 1953.
18. Waterhouse, Richard V., and Berendt, Raymond D.: Reverberation Chamber Study of the Sound Power Output of Subsonic Air Jets. Jour. Acoustic Soc. Am., vol. 30, no. 2, Feb. 1958, pp. 114–121.
19. Rollin, Vern G.: Effect of Jet Temperature on Jet-Noise Generation. NACA TN 4217, 1958.
20. Eldred, Ken: Noise Measurement of Four Rohr Aircraft Model Jet Nozzles. Rep. No. 238–11–1, Paul S. Veneklasen & Assoc., Los Angeles (Calif.), Mar. 14, 1958.
21. Howes, Walton L.: Ground Reflection of Jet Noise. NACA TN 4260, 1958.
22. Kamps, Edwin C.: Statistical Evaluation of Near-Field Sound Pressures Generated by the Exhaust of a High-Performance Jet Engine. Jour. Acoustic Soc. Am., vol. 31, no. 1, Jan. 1959, pp. 65–67.
23. Coles, Willard D., Mihaloew, John A., and Callaghan, Edmund E.: Turbojet Engine Noise Reduction with Mixing Nozzle-Ejector Combinations. NACA TN 4317, 1958.
24. Beranek, Leo L.: Acoustic Measurements. John Wiley & Sons, Inc., 1949.
25. Brand, Willem: Some Notes on the Practical Aspects of Noise Measurement and Analysis Using B&K Equipment. Brüel and Kjaer Tech. Rev., no. 4, 1955, pp. 1–7.
26. Hoeft, Lothar O.: A System for Measuring the High Sound Pressure Levels from Rockets. TR 56–655, WADC, Dec. 1956.
27. Deissler, Robert G.: Analytical and Experimental Investigation of Adiabatic Turbulent Flow in Smooth Tubes. NACA TN 2138, 1950.

TABLE I.—FAR-FIELD JET NOISE CHARACTERISTICS CONSIDERED BY VARIOUS INVESTIGATORS

Author and reference number	Type of jet	Total acoustic power		Acoustic-power spectrum		Directivity		Acoustic-pressure spectrum		Probability density	
		Subsonic	Supersonic	Subsonic	Supersonic	Subsonic	Supersonic	Subsonic	Supersonic	Subsonic	Supersonic
Fitzpatrick and Lee, 16	Air jets	X		X							
Lee, 17	Air jets	X		X		X		X			
Tyler and Perry, 10	Air jets and jet engines.	X	X	X	X	X	X	X	X		
Callaghan and Coles, 9	Air jets and jet engines.	X	X	X	X	X	X	X	X		
Clark, et al., 11	Jet engines	X	X	X		X	X	X	X		
Waterhouse and Berendt, 18	Air jets	X		X							
Cole, et al., 2	Rockets		X		X		X				
Rollin, 19	Air jet	X		X							
Eldred, 20	Air jet		X		X		X		X		
Present tests	Air jets	X	X	X	X	X	X	X	X	X	X

TABLE II. CHARACTERISTICS OF NOISE TESTS

	Author and reference number	Nozzle type	Nozzle-exit diameter, D, in.	Exit velocity, U, ft/sec	Method of determining jet velocity	Average exit temperature, °F
1	Fitzpatrick and Lee, 16	Parallel flow	0.765, 1.530	350–950	P/p_0, T	30.
2	Lee, 17	Straight pipe	0.625	230–840	$(P/p_0)_{max}$, T estimated, U_m from ref. 27.	20.
3	Tyler and Perry, 10	Bellmouth, convergent, convergent-divergent.	1, 2, 4, 7, 10 (Air jets), >10 (Engines).	770–1190 (Air jets), [a]~1850 (Engines).	[a]P/p_0, T	100. [a]1250.
4	Callaghan and Coles, 9	Convergent, convergent-divergent.	3, 4, 5 (Air jets), 19.75, 21.75 (Engines).	≈670–2600	P/p_0, T (air jets), $F/\dot{m}$ (jet engines).	200–1300.
5	Clark, et al., 11	Convergent	18–20	[a]1000–2600	$F/\dot{m}$ from engine parameters.	≈1300.
6	Waterhouse and Berendt, 18.	Bellmouth	0.5	450–930	P/p_0, T	30.
7	Cole, et al., 2	Convergent-divergent	Classified	Classified		Classified
8	Rollin, 19	Convergent	0.562	710–1550	P/p_0, T	80–1000.
9	Eldred, 20	Convergent	2.7	1860	P/p_0, T, and $F/\dot{m}$	977.
10	Present tests	Convergent	3, 5	680–1030	P/p_0, T	10.

[a] Estimated.

TABLE II.—Concluded. CHARACTERISTICS OF NOISE TESTS

	Surroundings	Measurement radius, r, ft	Included bandwidth, cps	Filter bandwidth	Type of signal averaging	Comments
1	Semireverberant chamber		≈350–13, 500	One-half octave	Mean square	Chamber open at top.
2	Free field (5 ft above ground).	3	36–13, 600	One-half octave	Mean square	Claims appreciable acoustic power above 13,600 cps.
3	Reverberant chamber		[a]≈100–16, 000	[a]Narrow, one-third octave, octave.	Full wave rectified (over-all); quasi-peak corrected to root mean square (spectra).	L based on jet density.
4	Free field (6–10 ft above grass or concrete).	50 (Air jets), 200 (Engines).	≈30–10, 000	One-third octave	Full wave rectified (over-all); quasi-peak (spectra).	Air jets and turbojet engines.
5	Free field (6–8 ft above concrete).	100, 200, 400	20–10, 000	Octave	Full-wave rectified	Turbojet engines, microphone windscreen used.
6	Reverberant chamber		75–9, 600	Octave	[a]Full wave rectified	
7	Free field (variable height above ground in static tests; 50, 100 ft above ground in flight rests).	100, 250, 450 (Static), >400 (Flight).	37. 5–9, 600	Octave	Quasi-peak	Static and flight tests of rockets, F = 1000–130,000 lb.
8	Free field (7 ft above concrete).	7	200–31, 500	One-third octave	Quasi-peak	High jet temperatures provided by heat exchanger.
9	Free field (0.75 ft above concrete).	12.5, 25, 50	225–54, 300	Octave	[a]Full wave rectified	
10	Free field (10 ft above grass).	50	20–20, 000	One-third octave	Full wave rectified (over-all); quasi-peak (spectra).	

[a] Estimated.

TABLE III.—TOTAL ACOUSTIC POWER CORRECTIONS

	Author and reference number	Velocity correction, db	Reflection correction, db	Wind correction, db	Frequency pass-band correction, db	Meter-averaging correction, db
1	Fitzpatrick and Lee, 16	[a]$<+0.5$	0	?	$<+0.5$	0
2	Lee, 17	0			+1.0	0
3	Tyler and Perry, 10	[a]$<+0.5$	0	?	+0.5	+1.0
4	Callaghan and Coles, 9	[a]$<+1.5$ ($D=3$ in.), [a]$<+1.0$ ($D=5$ in.), 0 (Engines).	[a]−1.5 (Air jets), [a]−0.5 (Engines).	−0.5 at min. L, 0 at max. L.	0	+1.0
5	Clark, et al., 11	0	0		0	+1.0
6	[illegible]	0			0	+1.0
7	Cole, et al., 2	Variety of conditions				→
8	Rollin, 19	[a]$>+1.5$	−0.8	0	0	−3.0
9	Eldred, 20	?	−3.0	0	0	[a]+1.0
10	Present tests	[a]$<+1.0$ ($D=5$ in.), +1.5 ($D=3$ in.).	[a]−1.5	0	0	+1.0

[a] Estimated.

U.S. GOVERNMENT PRINTING OFFICE: 1960

NASA TR R-52
National Aeronautics and Space Administration
SIMILARITY OF FAR NOISE FIELDS OF JETS. Walton L. Howes. 1960. i, 44 p. diagrs., photo., tabs. GPO price 50 cents. (NASA TECHNICAL REPORT R-52.)

Similarity parameters for far-field noise from subsonic and supersonic jets issuing from circular nozzles are derived and tested using experimental data. Relations for the total acoustic power, acoustic-power spectrum, acoustic directivity, local mean-square-pressure spectrum, and acoustic-pressure probability-density are considered. Subsonic data correlated well in all respects. With the exception of total-power similarity, supersonic data also correlated well. Subsonic and supersonic correlations generally differed only slightly.

Copies obtainable from Supt. of Docs., GPO, Washington

1. Noise (7.4)
I. Howes, Walton L.
II. NASA TR R-52

NASA

NASA TR R-52
National Aeronautics and Space Administration
SIMILARITY OF FAR NOISE FIELDS OF JETS. Walton L. Howes. 1960. i, 44 p. diagrs., photo., tabs. GPO price 50 cents. (NASA TECHNICAL REPORT R-52.)

Similarity parameters for far-field noise from subsonic and supersonic jets issuing from circular nozzles are derived and tested using experimental data. Relations for the total acoustic power, acoustic-power spectrum, acoustic directivity, local mean-square-pressure spectrum, and acoustic-pressure probability-density are considered. Subsonic data correlated well in all respects. With the exception of total-power similarity, supersonic data also correlated well. Subsonic and supersonic correlations generally differed only slightly.

Copies obtainable from Supt. of Docs., GPO, Washington

1. Noise (7.4)
I. Howes, Walton L.
II. NASA TR R-52

NASA

NASA TR R-52
National Aeronautics and Space Administration
SIMILARITY OF FAR NOISE FIELDS OF JETS. Walton L. Howes. 1960. i, 44 p. diagrs., photo., tabs. GPO price 50 cents. (NASA TECHNICAL REPORT R-52.)

Similarity parameters for far-field noise from subsonic and supersonic jets issuing from circular nozzles are derived and tested using experimental data. Relations for the total acoustic power, acoustic-power spectrum, acoustic directivity, local mean-square-pressure spectrum, and acoustic-pressure probability-density are considered. Subsonic data correlated well in all respects. With the exception of total-power similarity, supersonic data also correlated well. Subsonic and supersonic correlations generally differed only slightly.

Copies obtainable from Supt. of Docs., GPO, Washington

1. Noise (7.4)
I. Howes, Walton L.
II. NASA TR R-52

NASA

NASA TR R-52
National Aeronautics and Space Administration
SIMILARITY OF FAR NOISE FIELDS OF JETS. Walton L. Howes. 1960. i, 44 p. diagrs., photo., tabs. GPO price 50 cents. (NASA TECHNICAL REPORT R-52.)

Similarity parameters for far-field noise from subsonic and supersonic jets issuing from circular nozzles are derived and tested using experimental data. Relations for the total acoustic power, acoustic-power spectrum, acoustic directivity, local mean-square-pressure spectrum, and acoustic-pressure probability-density are considered. Subsonic data correlated well in all respects. With the exception of total-power similarity, supersonic data also correlated well. Subsonic and supersonic correlations generally differed only slightly.

Copies obtainable from Supt. of Docs., GPO, Washington

1. Noise (7.4)
I. Howes, Walton L.
II. NASA TR R-52

NASA